The Journal of Supercritical Fluids 130 (2017) xxx–xxx

Contents lists available at ScienceDirect

The Journal of Supercritical Fluids

journal homepage: www.elsevier.com/locate/supflu

Characterization of solid-fluid equilibrium regions of computed constant-overall-composition phase diagrams

Sabrina Belén Rodriguez-Reartes, Jorge A. Guapacha, Marcelo S. Zabaloy*

Planta Piloto de Ingeniería Química (PLAPIQUI), Departamento de Ingeniería Química (DIQ), Universidad Nacional del Sur (UNS)-CONICET, CC 717, 8000, Bahía Blanca, Argentina

ARTICLE INFO

Keywords:
Theoretical methods
Solid-Fluid equilibrium
Asymmetric binary systems
Equation of state
Solidified fraction
Miscibility islands

ABSTRACT

In this work we studied the features of the solid-fluid region of computed binary constant-overall-composition phase diagrams (COCPDs), by resorting to calculated constant solidified-fraction curves. As generally done for constant overall composition (COC) mixtures, we computed phase envelopes (made of fluid–fluid equilibrium (FFE) and solid-fluid equilibrium (SFE) segments), together with appropriate segments of solid-fluid–fluid equilibrium (SFFE) curves. Besides, for achieving a more complete characterization of solid-fluid regions of computed COCPDs, we calculated sets of constant solidified fraction curves. A methodology to find the quantitative connection among these curves and already computed SFFE lines is proposed. The results obtained for heterogeneous regions suggest the existence of complex patterns of behavior, for phase equilibria involving fluid and solid phases. Some of them could be regarded as unexpected. The proposed approach can be applied, in general, to binary systems which present precipitation, in pure form, of the heavy compound.

1. Introduction

The phase behavior over wide pressure ranges of binary systems made of a light compound (e.g., CO_2, CH_4, C_3H_8) and an organic compound having a relatively high molecular weight is of interest in a number of applications, e.g, Refs. [1–5]. Within the ranges of conditions of interest, these systems may present fluid–fluid (FFE), solid-fluid (SFE), liquid-liquid-vapor (LLVE) and solid-fluid–fluid (SFFE) equilibria. Typically, transition pressures (temperatures) are measured at set temperature (pressure), and set overall composition (COCPDs), through the synthetic method, covering a temperature (pressure) range. The result is a set of measured points (segments) of the phase envelope of the COCPD, eventually together with sets of points (segments) of three-phase equilibrium lines. This is shown in the pressure-temperature space. Appropriate models for these complex systems may be useful to interpolate and extrapolate experimental information, and to study possible patterns of phase behavior. One of such models has been used in Refs. [1–4].

An approach for describing solubilities of solids (SFE) at high pressures is the use empirical density-based correlations (EDBCs) [5,6]. They properly correlate existing solubility data in the pressure range from 10 MPa to 30 MPa [6]. EDBCs are based on the observation that, in the mentioned region, a double logarithmic plot (i.e., logarithm of the solubility vs. logarithm of the solvent density) yields a linear relationship [6]. However, the extrapolation of EDBCs beyond the mentioned limits fails (i.e., it fails at low temperatures or at very high pressures, where liquid-like densities appear) [6]. A list of the empirical approaches most used for modeling solubilities of solids in supercritical fluids can be found in ref [5].

EDBCs provide information about situations where a solid phase coexists with a fluid phase, but without giving information on the individual phases themselves. On the other hand, equations of state (EOSs) of the van der Waals family, e.g., the PR-EOS [7], give complete information for (mixed or pure) fluid phases; while (pure) solid fugacity equations (PSFugEs, [8–12]), e.g., the one used in this work (described in Section 3.1.1), do the same for solid phases made of pure compounds. From combining EOSs and PSFugEs it is possible to calculate all kinds of multiphase-multicomponent equilibria involving fluid and solid phases, except for those equilibria where solid solutions, i.e., solid phases not made of a single component, are present. A variety of EOSs may be used for describing the properties of supercritical fluid mixtures [5], e.g., Soave-Redlich-Kwong (SRK) EOS, Peng-Robinson (PR) EOS, group contribution (GC) EOS, perturbed hard-sphere chain (PHSC) EOS, quasi-chemical nonrandom lattice fluid (QLF) EOS, multifluid nonrandom lattice fluid (MF-NLF) EOS, etc [5]. Care should be exercised when choosing and EOS: sophisticated EOSs can yield an inconsistent behavior [13]. Attempts have been made of defining a single relationship between pressure, temperature, density and composition to

* Corresponding author.
E-mail addresses: mzabaloy@plapiqui.edu.ar, marcelo.santiago.zabaloy@gmail.com (M.S. Zabaloy).

http://dx.doi.org/10.1016/j.supflu.2017.07.010
Received 29 March 2017; Received in revised form 6 July 2017; Accepted 13 July 2017
Available online 25 July 2017
0896-8446/ © 2017 Elsevier B.V. All rights reserved.

Nomenclature

Symbols and acronyms

1st CEP	1st critical end point
2nd CEP	2nd critical end point
C_1, C_2, C_3	Constants that characterize the pure heavy component SLE curve
CEP	Critical end point
COC	Constant overall composition
COCPD	Constant-overall-composition phase diagram
DL	(vertical) dashed line
EDBC	Empirical density-based correlation
EOS	Equation of state
$\hat{f}_2(T, 1, \upsilon_o)$	Fugacity of the pure heavy component ("2"), in liquid state, at system T and P
$f_2^S(P, T, \upsilon_o)$	Fugacity of the pure heavy component ("2") in solid state at system T and P
FF	Fluid-fluid
FFE	Fluid–fluid equilibrium
FI	Full isopleth
GC-EOS	Group contribution EOS
HT	High temperature
I-C-FPF-L	**I**sopleth fluid–fluid **C**onstant **F**luid-**P**hase-**F**raction **L**ine
I-C-SPF-L	**I**sopleth solid-fluid **C**onstant **S**olid-**P**hase-**F**raction **L**ine
IE	**I**sopleth two-phase **E**nvelope
INE	**I**sopleth **N**on-**E**nveloping two-phase line
L	Liquid
LL	Liquid-liquid
LLE	LL equilibrium
LLV	Liquid-liquid-vapor
LLVE	LLV equilibrium
LT	Low temperature
MF-NLF-EOS	Multifluid nonrandom lattice fluid EOS
MPgAc	Medroxiprogesterone acetate
P	Absolute pressure
P_{crit}	Critical (absolute) pressure
%SMPgAc	Percentage of solidified heavy component (MPgAc)
PHSC-EOS	Perturbed hard-sphere chain EOS
PR-EOS	Peng-Robinson EOS
PSFugE	Pure solid fugacity equation
P_{tp}	Pure compound vapor-liquid equilibrium P at T_{tp} (consistently obtained from the PR-EOS)
PVT	Pressure-temperature-volume
QLF-EOS	Quasi-chemical nonrandom lattice fluid EOS
R	the universal gas constant
S	Solid
SF	Solid-fluid
SFE	SF equilibrium
SFF	Solid-fluid-fluid
SFFE	SFF equilibrium
SF-MD	Binary solid-fluid master diagram
SL	Solid-liquid
SLE	SL equilibrium
SLV	Solid-liquid-vapor
SLVE	SLV equilibrium
SLV-HT	High temperatur SLV locus
SLV-LT	Low temperature SLV locus
SRK-EOS	Soave-Redlich-Kwong EOS
SV	Solid-vapor
SVE	SV equilibrium
T	Absolute temperature
T_{crit}	Critical (absolute) temperature
TP	Triple point
tpd	Reduced tangent plane distance
T_{tp}	Triple point absolute temperature for the pure heavy compound
u_2	Mole fraction of component "2"
V	Vapor
υ_o	Pure heavy component molar volume in liquid state
υ_u	Molar volume of fluid phase of composition u_2
υ_x	Molar volume of fluid phase of composition x_2
w_2	Mole fraction of component "2" in the S phase
$w_{2,SLV}$	Mole fraction of component "2" in S phase at SLVE
x_2	Mole fraction of component "2" in the fluid phase
$x_{2,SLV}$	Mole fraction of component "2" in l phase at SLVE
$y_{2,SLV}$	Mole fraction of component "2" in V phase at SLVE
z_2	Overall composition (mole fraction of component "2") of the binary system

Greek letters

$\Delta\upsilon^{S-L}$	Solid-liquid molar volume difference ($\upsilon_{solid} - \upsilon_{liquid}$)
Φ_F	Fluid phase fraction (mole basis)
Φ_S	Solid phase fraction (mole basis)
Φ_S^L	Φ_S of SL system (at set z_2) under SLVE
Φ_S^V	Φ_S of SV system (at set z_2) under SLVE
ω	Acentric factor

describe simultaneously both, the fluid state and the solid state, e.g., ref [14].

In the present work we applied the PSFugE approach described by Prausnitz [10] and presented in more detail by Firoozabadi [9], but in the particular form of ref [2], to the calculation of the fugacity of the pure solid phase (see Section 3.1.1 for more details). Such form is continuous at the triple point temperature [12], and it can be applied, over wide ranges of pressure (or density), to multiphase equilibria involving pure solids coexisting with fluid mixtures.

With regard to the literature sources of high pressure experimental solid-fluid equilibrium data the reader may consult the comprehensive review in Ref. [5].

In previous works, we calculated COCPDs including the two-phase envelope and the appropriate segments of SFFE lines. The systems considered were CO_2 + medroxyprogesterone acetate (MPgAc) [2], CO_2 + progesterone [4] and CH_4 + n-triacontane [4]. On the other hand, only phase envelopes were computed in other works. In this last case the studied systems were CO_2 + Mitotane [1], C_3H_8 + n-eicosane [3] and CO_2 + n-eicosane [3]. In all cases [1–4], the phase envelopes included SFE and FFE segments. The systems in Refs. [1] and [2] present retrograde melting behavior. This is also the case for systems CO_2 + progesterone [4] and CO_2 + n-eicosane [3]. For a detailed description of retrograde melting behavior see Ref. [4].

As an illustrative example, Fig. 1 shows, for system CO_2(1) + MPgAc(2), a computed COCPD. The overall MPgAc mole fraction is $z_2 = 9.2404 \times 10^{-5}$. Fig. 1 depicts the calculated phase envelope (solid line) and it shows the appropriate segment of the calculated solid-liquid-vapor (SLV) line. This line characterizes, at least partially, the SFE region. The phase envelope has a single segment which is of the solid-fluid type. Based on the limited information it provides, the phase diagram of Fig. 1 has no FFE segments in its phase envelope, and, in principle, it would not have FFE regions either.

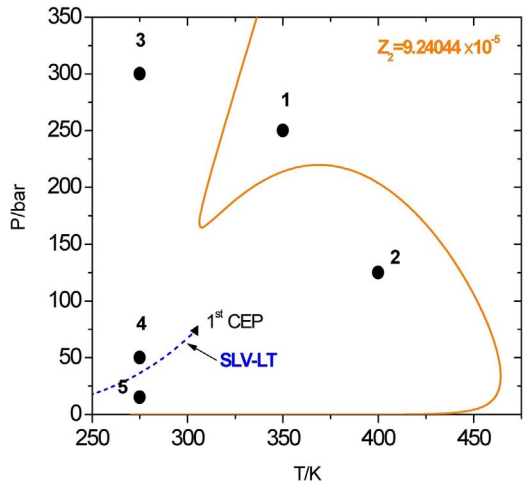

Fig. 1. Constant overall composition phase diagram (COCPD) for the CO_2(1) + MPgAc(2) mixture of global composition $z_2 = \ddot{z}_2 = 9.24044 \times 10^{-5}$. Solid line: Solid-fluid phase envelope. — solid-liquid-vapor (SLV-LT) curve. 1st CEP: first critical end point. Model parameters in Appendix A. The shown phase envelope has no segments of the FFE type.

Details about the model used to generate Fig. 1 and about its associated parameters, are given in Section 3.1. At any point on the SF boundary (solid line in Fig. 1) a fluid phase of composition equal to z_2 is at equilibrium with an incipient (differential size) solid phase, which in Fig. 1 has been considered to be only made of the pure heavy compound. This assumption is also used throughout this work. Any point on the SLV line (dashed line) is a three-phase equilibrium point involving the pure solid, a liquid phase and a vapor phase.

From the information available in Fig. 1, one tends to conclude that at point 1 the mixture is an homogenous fluid, while at points 2–5 there is an heterogeneous solid-fluid equilibrium with finite amounts of the phases, i.e., none of the phases has a differential size. The heterogeneous nature ascribed to points 2–5 would be confirmed by the addition of computed lines of constant solidified fraction (Φ_S) to Fig. 1. Clearly, the computation of such lines would provide a more complete characterization of the solid-fluid regions of COCPDs.

Thus, the goal of this work is to propose and illustrate a methodology to study the behavior of the solid-fluid regions of computed COCPDs (methodology which resorts to calculated constant solidified-fraction curves) for binary asymmetric systems, as described by a given adopted model, when the information on previously computed phase envelopes and solid-fluid–fluid equilibrium lines is already available. Constant solidified fraction curves have not been considered in the literature quoted above (i.e., in refs [1–4,12]). The calculation of such curves may unveil unexpected features of the heterogeneous region of the studied system. The methodology here developed is useful for computing with a high level of detail binary COCPDs involving SFE regions.

To illustrate the proposed approach, we take the CO_2 + medroxyprogesterone acetate (MPgAc) system as our case study. Even though it is not the purpose of this work to find ways of making models match experimental data, the model (described in Section 3.1), and associated parameter values, used to generate Fig. 1 and all the other results of this work, is able to reproduce the SFE experimental transition pressures of the CO_2 + MpgAc system within 4.5% (average deviation, [2]). We emphasize that the focus of this work is set on the computation of COCPDs together with the proper interpretation of the calculation results, and it is not set on the prediction or correlation of experimental information. Thus, it was not necessary to perform in this work any exhaustive study on the advantages and/or disadvantages of the particular model here chosen to illustrate the application of the proposed approach.

Some equilibrium lines, where the amount of a given phase is constant, are not considered in this work: they are the lines located within heterogeneous regions where only fluid phases are present (regions where solid phases are absent).

2. Types of phase equilibrium isopleths

The word "isopleth" means in this work "constant composition". This composition may be the overall composition of a mixture, or the composition of one of the phases at equilibrium.

In this work, we need to distinguish among different types of phase equilibrium isoptlehs as stated below. The distinction between the types in items [a] and [b] is subtle. The isopleth types are the following:

[a] **I**sopleth two-phase **E**nvelope (**IE**)

Examples of IEs are the solid line in Fig. 1, and the line labeled "0" in Fig. 6. The IE is a two-phase equilibrium line characterized by an overall composition (z_2 in this work) that equals the composition of one of the equilibrium phases (x_2 in this work). The phase for which this composition identity ($x_2 = z_2$) takes place is of the fluid type. This implies that the other phase is incipient, i.e., its size, or its amount relative to the amount of the other phase, tends to zero. An IE defines the threshold of heterogeneity for the set overall composition of the mixture. This is to say that the IE is the boundary between homogeneity and heterogeneity. The overall composition (z_2) is a variable present in the system of equations that describe the IE. This is also the case for the fraction of incipient phase (e.g., Φ_S), which is set equal to zero. The IE could also be named "constant overall composition two-phase envelope". The pressure temperature projection of a given IE is experimentally observable in the laboratory by using the synthetic method. The IE may have fluid–fluid segments and solid-fluid segments (e.g., in Fig. 12, solid red lines (SF) and dashed red lines (FF)).

[b] **I**sopleth **N**on-**E**nveloping two-phase line (**INE**)

The INE is a two-phase equilibrium line characterized by a fixed composition for one of the equilibrium phases. Such phase is of the fluid type for the goals of this work (its composition is x_2 in this work). Neither the overall composition of the mixture nor the relative amounts of the phases are set when computing an INE. This is because such variables are not related to this thermodynamic object, which we name INE.

In general, the INE is not a boundary between homogeneity and heterogeneity, i.e., it does not define in general the threshold of heterogeneity. This is indicated by the words "non-enveloping" in the naming of this type of isopleth.

A given point of a given INE is associated to certain overall composition range. Any overall composition that does not violate the restriction of mass conservation is compatible with such point. There is compatibility if the considered overall composition lies in between those of the two equilibrium phases of the chosen point. Two different points of the INE have different associated overall composition ranges.

A given INE has a special IE as limiting case for the variables that are common to both types of isopleths. This happens when the considered overall composition (z_2) that defines the IE equals the phase composition that defines the INE (x_2).

In general, INEs are not observable in the laboratory. This is because it is not experimentally possible to keep constant the composition of a phase in a range of conditions, if the phases are to have finite (non differential) sizes. In spite of this lack of experimental observability, the concept of INE is helpful in the context of this work.

A typical, surely well known, textbook diagram (see Fig. 10.1 in page 332 of Ref. [15]) shows, for a binary system, the bubble and dew pressure surfaces, with liquid or vapor phase compositions, and

temperature, as independent variables, with both surfaces cut by a vertical constant mole fraction plane. The curve resulting from the intersection between such plane and the surfaces is an INE. This is because neither the overall composition, nor the amounts of the phases, needed to be set for obtaining such curve. The INE has a dew segment and a bubble segment.

The INE could also be named constant phase-composition two-phase line.

[c] **I**sopleth solid-fluid **C**onstant **S**olid-**P**hase-**F**raction **L**ine (I-C-SPF-L)

Examples of I-C-SPF-Ls are lines labeled '0′ to '10′ in Fig. 6. The I-C-SPF-L is a solid-fluid equilibrium line at set solidified fraction (Φ_S) and set overall composition (z_2). Indeed, the solidified fraction is a variable related to this thermodynamic object, as it is the overall composition. The I-C-SPF-L has, in general terms, a segment of the IE as limiting case. This happens at zero solidified fraction. An example of such a limiting case is the IE segment labeled SF in Fig. 12. The I-C-SPF-L could also have the relatively longer name "constant overall-composition − constant solid-phase-fraction solid-fluid line".

[d] Isopleth fluid–fluid constant fluid-phase-fraction line (I-C-FPF-L)

This line is analogous to the I-C-SPF-L except that the phase equilibrium is of the fluid–fluid type, and it could also be named "constant overall-composition − constant fluid-phase-fraction fluid–fluid line". This type of isopleth is not considered in this work, except, in a way, when the fraction of one of the fluid phases tends to zero (IE), as it is the case for the FF line in Fig. 12. The rest of the I-C-FPF-Ls of Fig. 12 would be located within the region bounded by lines FF and part of the SLV-HT line.

[e] Full isopleth (FI)

In this work, we mean by "full isopleth" (FI) a constant overall composition phase equilibrium object (COCPD) made of the IE plus a number of I-C-SPF-Ls, I-C-FPF-Ls, liquid-liquid-vapor (LLV) lines (or segments) and solid-liquid-vapor (SLV) lines (or segments). An example of FI is Fig. 7, which has no equilibria of the fluid–fluid type and hence it has no I-C-FPF-Ls. Another example of FI is Fig. 12, which has a set of I-C-SPF-Ls, which are identified with Arabic numbers in Fig. 12, and it also has (not shown) I-C-FPF-Ls in the fluid–fluid region bounded by the FF lines and by part of the SLV-HT line. Besides, two different SLV lines are present in the FI of Fig. 12 (LT means 'low temperature' and HT means 'high temperature').

Table 1 summarizes the types and features of the isopleths or of the isopleth segments here considered.

There are other types of phase equilibrium isopleths which we do not need to consider in this work, e.g., the isopleth three-phase envelopes which can be found in ternary or higher isopleths [16].

3. Calculation of solid-fluid equilibria

3.1. Computation of a single binary solid-fluid equilibrium point when z_2 and Φ_s are not specified

For calculating a solid-fluid equilibrium point for an asymmetric binary system such as CO_2(1) + MPgAc(2), we impose the solid-fluid isofugacity condition for component "2", together with the constraints of uniform pressure and uniform temperature throughout the system. Once we establish an equation for calculating the fugacity of the pure solid as a function of temperature and pressure, and choose an equation of state (EOS) for calculating the component fugacities in the fluid phases; we can calculate SF equilibria. The EOS also makes possible to compute equilibria for multiple fluid phases, in the absence of solid phases.

The expressions we used in the present work for calculating fugacities in fluid and solid state are the same than those presented in refs [1–3]. For the sake of clarity, we repeat them here.

The system of equations to be solved to compute a SFE point (or a point of an INE, Table 1, lines 3 and 4), when z_2 and Φ_s are not

Table 1
Summary of types and properties of isoplehs or of isopleth segments relevant to the present work.

Row number	Isopleth type	Acronym	Segment type	Fluid-fluid equilibrium	Solid-fluid equilibrium	solid-phase fraction (Φ_S)	fluid-phase-fraction	Overall mixture composition (z_2)	Composition of 1st fluid phase (x_2)	Composition of 2nd fluid phase
1	Isopleth two-phase envelope	IE	fluid-fluid	Yes	No	N/A	zero for incipient phase/ unity for the other phase	set	equal to overall composition	not set
2	Isopleth two-phase envelope	IE	solid-fluid	No	Yes	zero	unity	set	equal to overall composition	N/A
3	Isopleth non-enveloping two-phase line	INE	fluid-fluid	Yes	No	N/A	not set	not set	set	not set
4	Isopleth non-enveloping two-phase line	INE	solid-fluid	No	Yes	not set	not set	not set	set	N/A
5	Isopleth fluid–fluid constant fluid-phase-fraction line	I-C-FPF-L	always fluid-fluid	Yes	No	N/A	set	set	not set	not set
6	Isopleth solid-fluid constant solid-phase-fraction line	I-C-SPF-L	always solid-fluid	No	Yes	set	set	set	not set	N/A
7	Full isopleth	FI	All of the previous isopleth types are present in a full isopleth except for the INE. Three-phase lines also contribute to FIs. A chart of a FI is a COCPD.							

Notes: The solid phase is considered to be made of a pure compound. N/A means "not applicable". I-C-FPF-Ls are not computed in this work.

specified, for a binary asymmetric mixture of components 1 (light) and 2 (heavy), when assuming that the solid phase is made of only the pure heavy compound (2), is the following:

$$\ln(P) = \ln[h_{PVT}(T, 1, \upsilon_o)] \tag{1}$$

$$\ln(P) = \ln[h_{PVT}(T, x_2, \upsilon_x)] \tag{2}$$

$$\ln[f_2^s(P, T, \upsilon_o)] = \ln[\hat{f}_2(T, x_2, \upsilon_x)] \tag{3}$$

In the above equations, $P = h_{PVT}(T, u_2, \upsilon_u)$ is the EOS relationship between the absolute temperature (T), the molar volume (υ_u), the composition (u_2 = mole fraction of component 2; subscript 2: heavy component), and the absolute pressure (P), at fluid state, where the function h_{PVT} corresponds in this work to the PR-EOS [7] (but any other EOS could, in principle, be used). $\hat{f}_2$ is the fugacity of component "2" in the fluid phase. $\hat{f}_2 = \hat{f}_2(T, u_2, \upsilon_u)$ corresponds to the same EOS that is defined by the function h_{PVT}. Variables x_2 and υ_x in Eqs. (2) and (3) are, respectively, the composition (i.e., mole fraction of component 2) and molar volume of the fluid phase; and υ_o is the pure heavy component molar volume, in liquid state, at T and P (notice that Eq. (1) sets a relationship among T, P and υ_o, i.e., Eq (1) implies that υ_o is not independent from T and P). In Eq. (3), $f_2^S(P, T, \upsilon_o)$ is the fugacity of the pure heavy component in solid state at system T and P. Section 3.1.1 provides details on the model used for computing $f_2^S(P, T, \upsilon_o)$.

The variables in the system of Eqs. (1) to (3) are P, T, υ_x, υ_o and x_2. Thus, this system of equations has two degrees of freedom [5 variables – 3 equations = 2]. To compute a single solid-fluid equilibrium point, e.g., P and T could be fixed and Eqs. (1) to (3) be solved for υ_x, υ_o and x_2.

Notice that both, the relative amounts of the phases at equilibrium (Φ_s) and the overall composition (z_2), are not variables of the system of Eqs. (1) to (3).

With regard to three-phase equilibria, in previous works [1,3] we presented the system of equations to be solved to build SFF equilibrium lines, for a binary asymmetric system of components 1 (light component) and 2 (heavy component), when assuming that the solid phase is only made of the pure heavy compound. The system of equations for calculating SFF equilibria arises from imposing the equality of component fugacities in all phases, as well as the uniformity of temperature and pressure throughout the heterogeneous system.

3.1.1. Fugacity of the pure heavy component in solid state

This section can be skipped at first reading if the details on the particular model used in this work, for computing the pure solid fugacity, are not of interest to the reader at this time.

$f_2^S(P, T, \upsilon_o)$ is given by the following equation:

$$f_2^S(P, T, \upsilon_o) = \hat{f}_2(T, 1, \upsilon_o)\exp(U) \tag{4}$$

The variable U is defined as follows:

$$U = \frac{\Delta\upsilon^{S-L}}{RT_{tp}}\left[C_1\left(1 - \frac{T_{tp}}{T}\right) + C_2\left(\frac{T_{tp}}{T} - 1 + ln\left(\frac{T}{T_{tp}}\right)\right) + C_3\left(\frac{T}{2T_{tp}} - 1 + \frac{T_{tp}}{2T}\right) + \frac{T_{tp}}{T}(P - P_{tp})\right] \tag{5}$$

In Eq. (4), $\hat{f}_2(T, 1, \upsilon_o)$ is the fugacity of the pure heavy component, in liquid state, at system T and P, and, consistently, it is also given in this work by the PR-EOS [7]. We developed Eq. (4) from clear assumptions about the temperature dependency of the solid-liquid heat capacity difference. The derivation that led to Eq. (4), is based on the one available in Refs. [3,9]. In Eq. (5), the constants T_{tp}, P_{tp}, $\Delta\upsilon^{S-L}$, C_1, C_2 and C_3 correspond to the pure heavy component (component 2). T_{tp} is the triple point absolute temperature of the pure heavy compound, and P_{tp} is the pure compound vapor-liquid equilibrium pressure at the triple point temperature T_{tp} (consistently obtained from the PR-EOS). $\Delta\upsilon^{S-L}$ is the solid-liquid molar volume difference ($\upsilon_{solid} - \upsilon_{liquid}$). Constants C_1, C_2 and C_3characterize the pure heavy component solid-liquid equilibrium curve (melting curve, [2,3]). Such curve is obtained by setting $U = 0$ in Eq. (5) and by subsequently solving the resulting equation for P (as a function of T). R is the universal gas constant.

Eq. (5) was obtained in ref. [17] by extending a derivation available in Ref. [9] to the case of a solid-liquid heat capacity difference set as a linear function of temperature. See the detailed derivation of Eq. (5) in Appendix B (supplementary material) of Ref. [17].

3.2. Computation of a solid-fluid segment of an INE

To calculate a single solid-fluid equilibrium point of an INE (line 4, Table 1), x_2 is set at the desired value. This is also done for another variable, say variable T. Next, Eqs. (1) to (3) are solved for υ_x, υ_o and P. This computation is repeated at other values of T, thus covering a temperature range. The result is an INE. Typically, the variables chosen for generating a plot of the INE are P and T, i.e., the usually visualized INE projection is the $P - T$ projection.

Actually, due to the potential presence of turning points in the INEs, the specification of the second degree of freedom (the first is defined as x_2 = const.) often involves a change in the specified variable. Turning points are those where one of the variables of the set [υ_x, υ_o, P, T] is either locally maximum or locally minimum.

Before computing a solid-fluid segment of an INE, its endpoints are obtained. This is done by first calculating the stable parts of the binary SFF lines, according to, e.g., Refs. [1–3]. The endpoints of the INE SF segment are the SFFE points for which one of the fluid phases has a composition equal to the phase composition that specifies the INE. This is explained in detail later in this manuscript. Notice that a solid-fluid segment of a computed binary INE might not have endpoints at all, as long as the model does not allow the light component to solidify.

3.3. Computation of a full INE

The basic strategy for building a full INE (lines 3 and 4 of Table 1) consists of generating the SF segments (line 4, Table 1) and next of calculating, according to ref [18], the fluid–fluid equilibrium segments (line 3, Table 1) of the INE.

Fluid-fluid segments of INEs have as their endpoints stable LLV points and/or critical points [18], and/or SFF points (e.g., FF line in Fig. 12). Sometimes they have no endpoints, i.e., they connect in a continuous way dew segments, bubble segments and liquid–liquid segments.

3.4. Computation of a solid-fluid equilibrium point at set overall composition z_2 and set solid-phase fraction Φ_S

This subsection is about the computation of a point of a I-C-SPF-L (line 6, Table 1). The system of equations is in this case made in part by Eqs. (1) to (3). This is because the solid-fluid equilibrium condition is to be met. The equations to be added are the following ones:

$$z_2 = \Phi_S w_2 + \Phi_F x_2 \tag{6}$$

$$\Phi_S + \Phi_F = 1 \tag{7}$$

$$w_2 = 1 \tag{8}$$

Variable z_2 is the overall composition (mole fraction of component 2) of the binary heterogeneous system. z_2 defines the FI under study (Table 1, line 7).

Φ_S is the phase mole fraction of the solid phase, i.e., Φ_S is the number of moles present in the solid phase when the total number of moles in the heterogeneous system equals unity. Φ_F is the phase mole fraction of the fluid phase. As previously stated, x_2 is the mole fraction of component "2" in the fluid phase at solid-fluid equilibrium, and w_2 is the mole fraction of component "2" in the solid phase. Eq. (6) is the mass conservation restriction for component 2 and Eq. (7) is the overall mass balance. Eq. (8) restricts the solid phase to be made of only the pure heavy component.

The variables of the system of Eqs. (1) to (8) are nine, i.e, P, T, υ_x, υ_o, x_2, z_2, Φ_S, Φ_F and w_2; and the number of equations is six. Thus, the number of degrees of freedom is three. In this work, we spend them by setting the values of z_2 and Φ_S and of some other variable, such as P, to calculate a point of the curve of line 6 of Table 1. Since Eq. (8) is autonomous, a degree of freedom cannot be spent by setting the value of variable w_2.

3.5. Computation of an I-C-SPF-L

This corresponds to Table 1, line 6. This line is obtained by setting the desired values for z_2 and Φ_S in system (1) to (8), and by allowing a third variable, e.g., temperature T, to vary within a given range of values. At each value of T, system (1) to (6) is solved for the remaining six variables.

System (1) to (6), as previously stated, has three degrees of freedom. This means that this system defines six, out of its nine variables, as functions of the remaining three variables. In particular, system (1) to (6) can be considered to define the variable Φ_S as a function of variables z_2, T and P. Consequently, variable Φ_S is a function of T and P at set z_2 [$\Phi_S(T, P, z_2 = K)$]. The geometrical representation of $\Phi_S(T, P, z_2 = K)$ is a surface in the 3D space. If a constant value is set for Φ_S, i.e., if $\Phi_S = K'$, then, a curve of constant Φ_S becomes defined, i.e.,

$$K' = \Phi_S(T, P, z_2 = K) \tag{9}$$

The previous equation has two variables, i.e., T and P. It therefore defines a line in the T, P plane. Such line is said to be a contour line of level K' of function Φ_S; or a level K' contour line of function Φ_S (in both cases at a set overall composition z_2 equal to K). In this work we use the pairs of words 'contour line' and "level curve" as synonyms. We also use the words 'constant quality lines' to refer to constant Φ_S contour lines.

What we have named 'full isopleth' (Table 1, line 7) is in part a set of constant Φ_S contour lines, including $\Phi_S = 0$ lines (i.e., including SF segments of the isopleth two-phase envelope (IE, Table 1, line 1)). The other part of the full isopleth is made of fluid–fluid constant fluid-phase-fraction lines (Table 1, line 5).

Notice that, by considering the Eqs. (1) to (8) it is possible to calculate any level curve, from $\Phi_S = 0$ (isopleth phase envelope) to $\Phi_S = \Phi_{S,max}$ ($\Phi_{S,max}$ equals z_2: this is discussed in the following section).

3.6. Relationship among z_2, x_2 and Φ_s

From Eqs. (6) to (8), we write,

$$z_2 = x_2 + \Phi_S - x_2\Phi_S \tag{10}$$

From looking at Eq. (10), we conclude that z_2 is a symmetric (quadratic) function of x_2 and Φ_S since z_2 is invariant under the permutation of variables x_2 and Φ_S. Eq. (10) implies that

$$\Phi_S = \frac{z_2 - x_2}{1 - x_2} \tag{11}$$

and also that

$$x_2 = \frac{z_2 - \Phi_S}{1 - \Phi_S} \tag{12}$$

At set z_2 Eq. (11) defines Φ_S as a non linear function of x_2. If Φ_S is computed in the range for x_2 from zero to unity, for a set value of z_2, and if only the points with $\Phi_S \geq 0$ are kept, then, a line as those shown in Fig. 2 is obtained.

Notice that Fig. 2 is the consequence of two restrictions: mass conservation (Eqs. (6) and (7)) and purity of the solid phase (Eq. (8)). Fig. 2 does not depend on the choice of models for the fugacities and PVT relationships in the fluid and solid phases.

As an example, the progress of the solidification process at $z_2 = 0.6$ (see Fig. 2) is from point A ($x_2 = 0.6, \Phi_S = 0$) to point B ($x_2 = 0, \Phi_S = 0.6$). At point A the heavy component is completely solubilized in the fluid phase ($\Phi_S = 0$). As the solidification progresses, the amount of heavy component in the fluid phase decreases (i.e., x_2 decreases, along the $z_2 = 0.6$ curve in Fig. 2) up to a point where no more heavy component is left in the fluid phase ($x_2 = 0$, point B, complete depletion of the fluid phase, in favor of the solid phase). We see in curve AB that $x_{2_{max}} = 0.6 = z_2$ (point A) and that $\Phi_{S_{max}} = 0.6 = z_2$ (point B) while their minimum values are $x_{2_{min}} = 0$ (point B) and $\Phi_{S_{min}} = 0$ (point A). Fig. 2 shows that without loss of generality the following restrictions apply to every curve in Fig. 2:

At set z_2:

$$0 \leq x_2 \leq z_2 \tag{13}$$

$$z_2 \geq \Phi_S \geq 0 \tag{14}$$

Eqs. (13) and (14) are written in this way to mean the following: when x_2 is at its minimum (zero), then, Φ_S is at its maximum (z_2); and vice versa.

It is interesting to observe, from Eq. (12), that a two-phase solid-fluid equilibrium line of constant overall composition z_2 and constant solidified fraction Φ_S (Table 1, line 6) presents a unique fluid phase composition x_2 throughout the whole line. This can be also graphically seen: if, e.g., $\Phi_S = 0.4$ is set in Fig. 2 (dashed horizontal line) for $z_2 = 0.7$, then, a value of x_2 equal to approximately 0.5 is read, and this is the only x_2 value provided by Fig. 2 at the set Φ_S and z_2. The phase densities (mainly that of the fluid phase) do vary along the level curve.

3.7. Identification of constant Φ_S curves reaching a given solid-fluid–fluid equilibrium point

As done in previous works for binary systems (e.g., Ref. [3]), before computing two-phase equilibria we calculate all the three-phase equilibrium lines. In particular we compute the three-phase lines involving a solid phase [solid-fluid–fluid (SFF) equilibrium lines].

This previous knowledge of the binary SFF lines is, among other

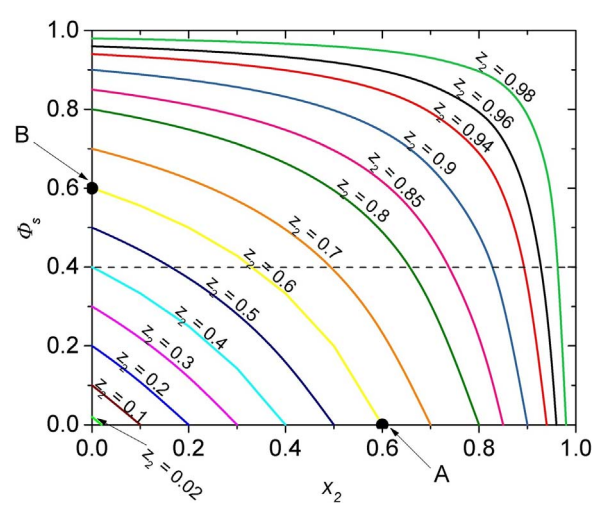

Fig. 2. Coexistence of a pure solid phase and a fluid phase for a binary system. Solidified fraction Φ_S as a function of the fluid phase composition x_2, at set overall composition z_2, for a range of z_2 values. See Eq. (11).

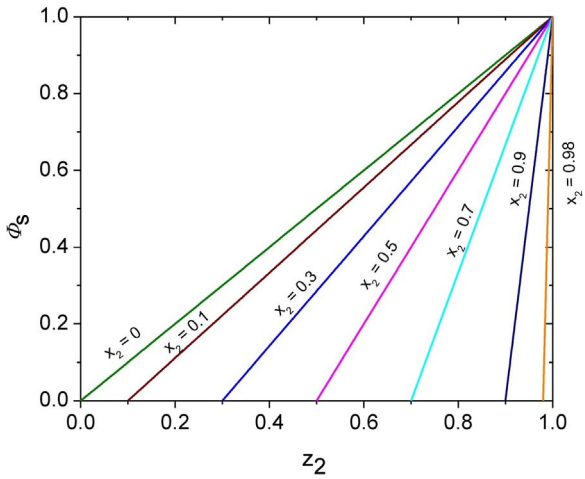

Fig. 3. Coexistence of a pure solid phase and a fluid phase for a binary system. Solidified fraction Φ_S as a function of the overall composition z_2 at set fluid phase composition x_2, for a range of x_2 values. See Eq. (11).

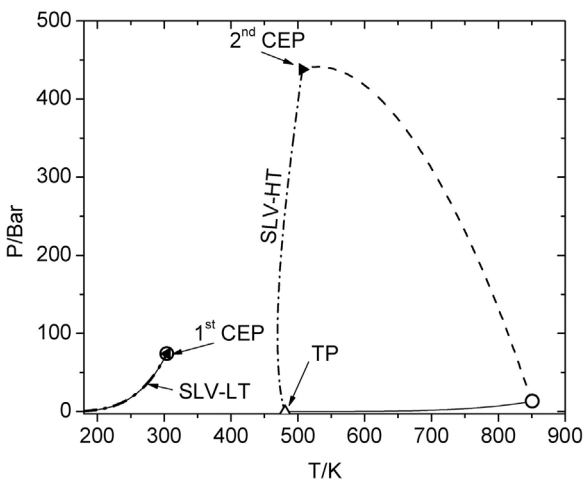

Fig. 4. Pressure(P)-Temperature(T) projection of calculated univariant lines for the system CO_2(1) + MPgAc(2). Dahed line: Critical loci. Solid line: pure compound saturation curve (vapor-liquid). Dashed-dotted line: solid-liquid-vapor (SLV-LT and SLV-HT) curves. ○: pure compound critical point. Δ: pure compound triple point (TP). ◄ 1st CEP: first critical end point. ► 2nd CEP: second critical end point. Model parameters in ndstAppendix A. The predicted phase behavior corresponds to TYPE F [19].

things, useful to establish, for a given computed SFF point, how many level curves have such point as their endpoint, and which are the Φ_S values corresponding to such curves. Having this been said, the reader may jump to Section 3.8 without loss of continuity and return to what remains of this section later.

In this work we have selected the case of the binary system CO_2 + MPgAc to illustrate how the solid-fluid region is studied for a set of overall mixture compositions. The parameters used in the model (previously described), which characterize the phase behavior of this system, are taken from Ref. [2]. In such work [2], a good reproduction of experimental phase equilibrium information was obtained. We report the values of the pure compound properties and of other parameters in Appendix A.

The system CO_2 + MPgAc has a predicted phase behavior of type F [1,2,19]. In Fig. 4, we show the computed characteristic map of the phase-behavior of system CO_2 + MPgAc in its PT projection. This map is made of a number of univariant lines.

We see in Fig. 4 two solid-liquid-vapor (SLV) curves (dashed-dotted lines). One of them, starts at the 1st critical end point (1st CEP) and extends towards low temperatures (SLV-LT line). The other curve (SLV-HT), stems from the triple point (TP) of pure medroxiprogesterone acetate and ends at the 2nd critical end point (2nd CEP). In each CEP a critical phase coexists with a pure MPgAc solid phase. Fig. 4 also shows the computed pure-compound vapor pressure curves (solid lines), binary critical lines (dashed curves), MPgAc triple point (TP), and critical points of the pure compounds (empty circles). At the scale of Fig. 4, it is not possible to visualize the (short) critical line which connects the CO_2 critical point (at about 304 K) and the 1st CEP. Besides, the pure CO_2 vapor-liquid equilibrium curve has, at the scale of Fig. 4 practically the same PT projection than the SLV-LT line.

The existence of computed SLV points with no solid CO_2 at arbitrarily low temperatures (SLV-LT line) is due to the fact that we have not allowed the model to access the solid state for CO_2 (only MPgAc is allowed to precipitate).

In Fig. 5 we present the pressure-composition projection of the calculated SLV curves. Fig. 5 makes possible to read, at set pressure, the compositions of the phases at SLV equilibrium. The solid phase is always located in the vertical line at unity MPgAc mole fraction. A binary SLV point has a single degree of freedom. Thus, once the pressure is set, then, the temperature becomes defined. It can be seen in Fig. 4 at, say, 25 bar, that the corresponding SLV-LT point has a temperature different (lower) from that of the corresponding SLV-HT point. In Fig. 5, the curves indicated with a solid line describe the liquid (L) phase at SLV equilibrium, while the SLV-LT vapor curve is indicated with a dashed line and the SLV-HT vapor curve with a dashed-dotted line.

To identify the level curves that reach an already computed SFF point, we in a way compare, by using Eq. (11), the compositions of fluid phases of the SFF point with the overall composition of the binary system. Let us name, for a specific SFF point, the liquid, vapor and solid compositions $x_{2,SLV}$, $y_{2,SLV}$ and $w_{2,SLV}$, respectively. Indeed, in this work, $w_{2,SLV}$ equals unity. The procedure is as follows:

[a] Set the desired value of the overall composition z_2

[b] Choose an already computed SFF point (with fluid phase compositions $x_{2,SLV}$ and $y_{2,SLV}$)

[c] Set $x_2 = x_{2,SLV}$

[d] Using Eq. (11) compute Φ_S and set $\Phi_S^L = \Phi_S$

[e] If $\Phi_S^L > 0$, then, a curve of level Φ_S^L originates at the chosen SFF point. This curve has a solid-liquid nature at such SFF point.

[f] If $\Phi_S^L < 0$, then, no solid-liquid curve originates at the chosen SFF point.

[g] Set $x_2 = y_{2,SLV}$.

[h] Using Eq. (11) compute Φ_S and set $\Phi_S^V = \Phi_S$

[i] If $\Phi_S^V > 0$, then, a solid-vapor curve of level Φ_S^V originates at the chosen SFF point.

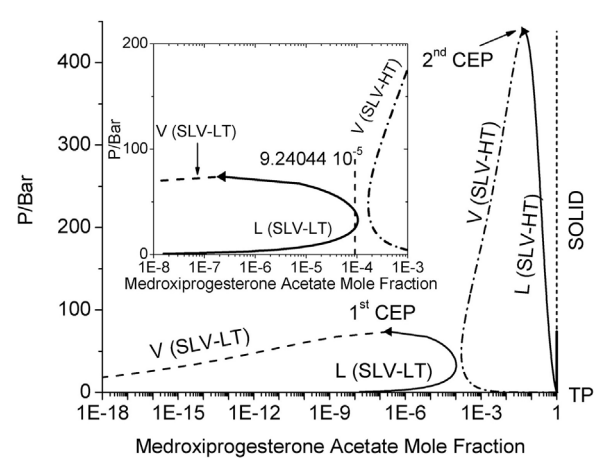

Fig. 5. Pressure-Composition projection of calculated solid-liquid-vapor (SLV-LT and SLV-HT) equilibrium curves for the system CO_2(1) + MPgAc(2). SLV curves as in Fig. 4. V: vapor phase. The solid phase is made of pure MPgAc. L: liquid phase. Model parameters in Appendix A. The insert is a zoom of the SLV curves which also shows a vertical dashed line of composition $x_2 = 9.24044 \times 10^{-5}$.

Table 2
Identification of level curves reaching a SFF point for the system $CO_2(1)$ + MPgAc(2) with model parameters from Appendix A.

Computed SLV points						$z_2^{'} = 1.4 \times 10^{-4}$ (Figs. 6 and 7)		$z_2^{''} = 9.24044 \times 10^{-5}$ (Fig. 9)	
Points	T/K	P/bar	$x_{2,SLV}$	$y_{2,SLV}$	$w_{2,SLV}$	Φ_S^L	Φ_S^V	Φ_S^L	Φ_S^V
1[1]	271.4899	33.2132	1.0444×10^{-4}	3.1810×10^{-15}	1	3.5560×10^{-5}	1.4000×10^{-4}	-1.2041×10^{-5}	9.2404×10^{-5}
2[1,a]	304.2142	73.8351	2.2867×10^{-7}	2.2867×10^{-7}	1	1.3977×10^{-4}	1.3977×10^{-4}	9.2175×10^{-5}	9.2175×10^{-5}
3[1]	253.1355	19.5184	6.8212×10^{-5}	2.3840×10^{-18}	1	7.1793×10^{-5}	1.4000×10^{-4}	2.4194×10^{-5}	9.2404×10^{-5}
4[2]	469.5956	97.3305	4.3285×10^{-1}	2.6599×10^{-4}	1	-7.6294×10^{-1}	-1.2602×10^{-4}	$-7.6303\ 10^{-1}$	-1.7363×10^{-4}
5[2,b]	506.7739	438.0743	5.0080×10^{-2}	5.0080×10^{-2}	1	-5.2573×10^{-2}	-5.2573×10^{-2}	-5.2623×10^{-2}	-5.2623×10^{-2}
6[2]	481.0000	4.3370×10^{-3}	$9.999999996 \times 10^{-1}$	9.9999636×10^{-1}	1	-2.4627×10^{9}	-2.7476×10^{5}	-2.4628×10^{9}	-2.7477×10^{5}

Computed SLV points						$z_2^{'''} = 9 \times 10^{-5}$ (Fig. 11)		$z_2^{''''} = 0.25$ (Figs. 12 and 13)	
Points	T/K	P/bar	$x_{2,SLV}$	$y_{2,SLV}$	$w_{2,SLV}$	Φ_S^L	Φ_S^V	Φ_S^L	Φ_S^V
1[1]	271.4899	33.2132	1.0444×10^{-4}	3.1810×10^{-15}	1	-1.4445×10^{-5}	9.0000×10^{-5}	2.4992×10^{-1}	2.5000×10^{-1}
2[1,a]	304.2142	73.8351	2.2867×10^{-7}	2.2867×10^{-7}	1	8.9771×10^{-5}	8.9771×10^{-5}	2.5000×10^{-1}	2.5000×10^{-1}
3[1]	253.1355	19.5184	6.8212×10^{-5}	2.3840×10^{-18}	1	2.1790×10^{-5}	9.0000×10^{-5}	2.4995×10^{-1}	2.5000×10^{-1}
4[2]	469.5956	97.3305	4.3285×10^{-1}	2.6599×10^{-4}	1	-7.6303×10^{-1}	-1.7603×10^{-4}	-3.2239×10^{-1}	2.4980×10^{-1}
5[2,b]	506.7739	438.0743	5.0080×10^{-2}	5.0080×10^{-2}	1	-5.2625×10^{-2}	-5.2625×10^{-2}	2.1046×10^{-1}	2.1046×10^{-1}
6[2]	481.0000	4.3370×10^{-3}	$9.999999996 \times 10^{-1}$	9.9999636×10^{-1}	1	-2.4628×10^{9}	-2.7477×10^{5}	-1.8473×10^{9}	-2.0610×10^{5}

[1] SLV points that belong to the SLV-LT three phase locus (Figs. 4 and 5).
[2] SLV points that belong to the SLV-HT three phase locus (Figs. 4 and 5).
[a] 1st CEP.
[b] 2nd CEP.

[j] If $\Phi_S^V < 0$, then, no solid-vapor curve originates at the chosen SFF point.

In some calculations, it is useful to let the algorithms work using a negative amount of a given phase [20].

3.7.1. Examples of application of steps [a] to [j]

What follows provides, for illustration purposes, examples on the application of the recipe given by steps [a] to [j]. However, the reader may now prefer to go directly to Section 3.8 and come back later to this point, if needed.

To fix ideas, for CO2 + MPgAc, we consider six different already computed SFF points and four values of the overall mixture composition z_2, i.e., z_2', z_2'', z_2''' and z_2''''. Then, we calculate Φ_S, for $x_2 = x_{2,SLV}$ and for $x_2 = y_{2,SLV}$ thus obtaining the Φ_S^L and Φ_S^V values as already explained. Table 2 presents the solidified fraction values obtained for the selected SFF points and set z_2 values. Notice that the results are reported showing a large enough number of digits to facilitate the reproduction of the computations by those readers interested in doing so. For the concentrations $x_{2,SLV}$ and $y_{2,SLV}$ of point 6 in Table 2 the shown number of digits is particularly large. This makes possible to conclude that the model tells that the liquid phase is more concentrated in the heavy component than the vapor phase, as expected. It would not have been possible to confirm or reject this expectation if $x_{2,SLV}$ and $y_{2,SLV}$ had been reported using less than 5 significant digits. All the calculations have been programmed in FORTRAN. Double precision accuracy was set for all computations. This level of accuracy is needed for the extremely sensitive computations performed in this work. This sensitivity shows itself in all its magnitude in Fig. B1 of Appendix B, where the phase condition changes twice in response to a pressure change of less than 0.01 bar. Besides, all positive variables where logarithmically scaled for solving the non-linear systems of equations.

In Table 2, points 1–3 are SLV points of the SLV-LT line (Fig. 5); and points 4–6 belong to the SLV-HT curve (Fig. 5). We see both, positive and negative values for Φ_S. A positive Φ_S value implies that the corresponding level curve (or a branch of it) exists in the heterogeneous region of the FI considered (e.g., branch 6 in Fig. 6) and originates at the considered SV equilibrium or SL equilibrium of the SLV point. Whereas a negative Φ_S value indicates that no level curve (or a branch of it) originates at such SV or SL equilibrium. This is so in spite of the fact that the INE associated to $x_2 = x_{2,SLV}$ or to $x_2 = y_{2,SLV}$ is always calculable. See as an example that there is no level "1" branch in Fig. 6 originating at a SLV point.

In Table 2, for the SLV-LT point 1 and:

[*i*] $z_2' = 1.4 \times 10^{-4}$ (Figs. 6 and 7), we obtain $\Phi_S^L > 0$ and $\Phi_S^V > 0$, then, both level curve branches contribute to the heterogeneous region of the FI with overall composition $1.4\ 10^{-4}$ and they stem from point 1.

[*ii*] $z_2'''' = 0.25$ (Figs. 12 and 13), we have again, $\Phi_S^L > 0$ and $\Phi_S^V > 0$. Thus, we arrive to a conclusion analogous to that of item [*i*]

[*iii*] z_2''=9.24044 × 10^{-5} (Fig. 9), we obtain $\Phi_S^L < 0$ and $\Phi_S^V > 0$. Thus, the level curve branch with $\Phi_S^V > 0$ will contribute to the heterogeneous region (starting at point 1 as a solid-vapor curve). However, the level curve with negative solidified fraction cannot contribute to the FI heterogeneous region, due to its impossible existence.

[*iv*] $z_2''' = 9.10^{-5}$ (Fig. 11), we also get $\Phi_S^L < 0$ and $\Phi_S^V > 0$, so, the conclusion is similar to that of item [*iii*].

In conclusion, the role of a given SLV point in a FI depends on the overall composition of the binary system.

In Table 2, for points 2 and 3, both solidified fractions remain positive (i.e. $\Phi_S^L > 0$ and $\Phi_S^V > 0$) for the four mixtures analyzed, i.e., for all z_2 values. From comparing the solidified fraction values of point 1, with those of points 2 and 3, we conclude that, for a given overall composition z_2, the signs of the computed solidified fractions depend in general on the chosen SLV point.

Points 4 to 6 belong to the SLV-HT curve and they have $\Phi_S^L < 0$ and $\Phi_S^V < 0$ for the mixtures with global compositions z_2', z_2'' and z_2'''. Then, the corresponding level curve branches supposedly stemming from the SLV-HT curve do not exist.

For the case of the mixture with $z_2'''' = 0.25$, we obtain that the level curve branches of point 6 do not exist because $\Phi_S^L < 0$ and $\Phi_S^V < 0$. The same occurs, at z_2'''', for the point 4 solid-liquid level curve branch ($\Phi_S^L < 0$); but not for the point 4 solid-vapor level curve branch ($\Phi_S^V = 2.4980.10^{-1} > 0$) which originates at point 4. Finally, point 5 has $\Phi_S^L > 0$ and $\Phi_S^V > 0$ for the mixture with z_2'''' overall composition; then, both level curve branches stemming from point 5 contribute to the z_2''''FI.

We stress that the number of level curve branches having a specific SLV point as its origin depends on the overall composition z_2 of the FI.

3.8. Identfication of the appropriate segments of solid-fluid–fluid equilibrium (SFFE) curves for a specific FI

A given already computed solid-liquid-vapor equilibrium point contributes to the heterogeneous region of a computed FI of overall composition z_2 if $y_{2,SLV} < z_2 < w_{2,SLV} = 1$. Otherwise, the mass conservation principle would be violated. For instance, in Fig. 1, we have that $z_2 = 9.24044 \times 10^{-5}$. This composition is indicated in the insert of Fig. 5 as a dashed vertical line. Such line is located to the left of the SLV-HT locus, i.e., $z_2 = 9.24044 \times 10^{-5} < y_{2,SLV-HT}$ for every SLV-HT point. Thus, no point of the SLV-HT line contributes to the FI of Fig. 1. On the other hand, from Fig. 5, $y_{2,SLV-LT} < z_2 = 9.24044 \times 10^{-5} < w_{2,SLV-LT} = 1$ for every point of the SLV-LT locus. Thus, the whole SLV-LT line contributes to the heterogeneous region of the FI of $z_2 = 9.24044 \times 10^{-5}$, as shown in Fig. 1.

4. Results and discussion

4.1. FI of z_2 = 0.00014

Fig. 6 shows the calculated constant quality curves (i.e, level curves) for the z_2 = 0.00014 isopleth of system CO_2(1) + MPgAc(2). Fig. 6 is a full isopleth (FI). The labels in Fig. 6 are defined in Table 3. In Table 3 (as in Tables 4–6), the level of solidification is labeled using an Arabic number. The higher this number the higher the amount of solidified MPgAc, except only for the cases of levels 11 and 12 in Table 3. In this table a regular integer number and a primed integer number of equal value (e.g., 2 and 2′) correspond to separated branches of the same level curve. Notice that in Tables 3–6, the calculated percentage of solidified MPgAc (%SMPgAc) in the mixture is reported for every label (instead of the Φ_S value). This is the number of moles of solid MPgAc relative to the

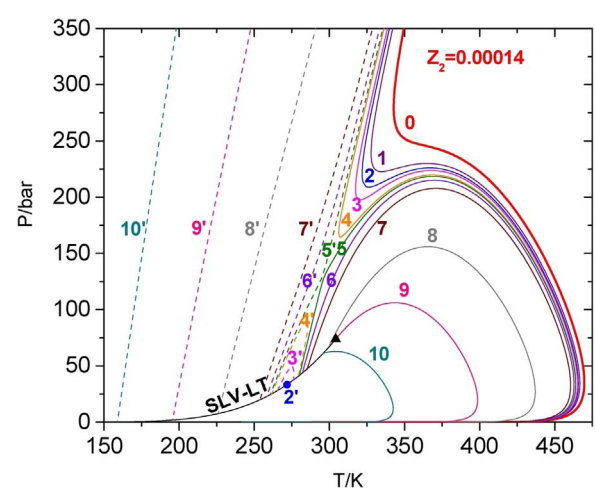

Fig. 6. Computed full isopleth (FI, Table 1, line 7) showing SF constant quality curves (Table 1, line 6). System: CO_2(1) + MPgAc(2) mixture of global composition $z_2 = z_2'$= 0.00014 and z_1 = 0.99986. Labels: see Table 3. Model parameters in Appendix A.

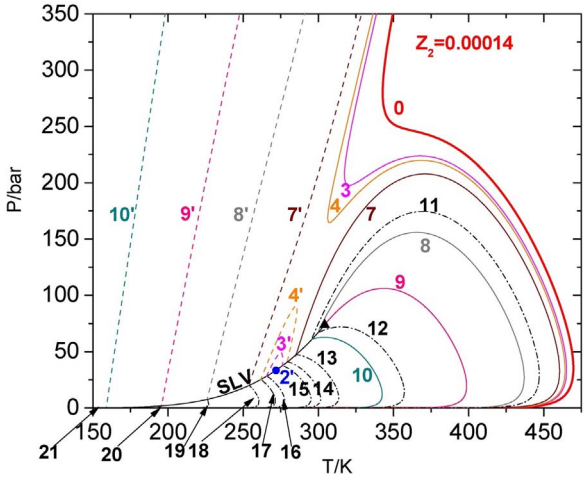

Fig. 7. This figure corresponds to the same isopleth of Fig. 6, but it shows pairs of SF level curves that originate at the same SLV point (e.g., the pair of curves with levels 10 and 11). Labels: see Table 3.

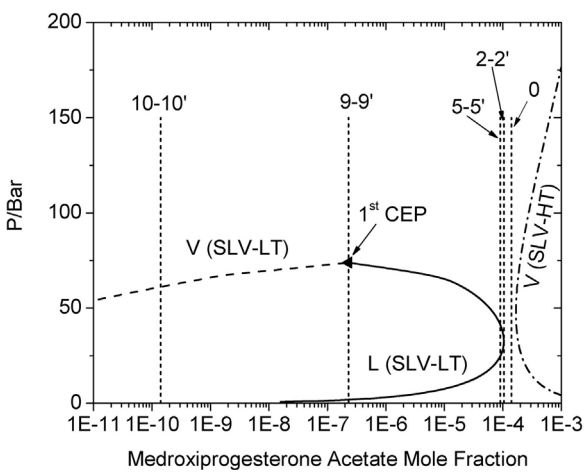

Fig. 8. Pressure-Composition projection of Fig. 5 shown in the low MPgAc concentration range. SLV curves as in Figs. 4 and 5. The vertical straight lines correspond to some of the level curves of Figs. 6 and 7 and to Table 3. From left to right, the INEs MPgAc mole fractions (x_2) of the vertical straight lines are: $x_2 = 1.40017 \times 10^{-10}$ (i.e., level 10-10′ in Table 3), $x_2 = 2.28670 \times 10^{-7}$ (9-9′), $x_2 = 9 \times 10^{-5}$ (5-5′), $x_2 = 1.04444 \times 10^{-4}$ (2-2′) and $x_2 = 1.4\ 10^{-4}$ (0-0′). The level (9-9′) x_2 value equals the composition of the critical phase of the 1st CEP.

total number of moles of MPgAc present in the system, in percent basis, and it is obtained as:

$$\%\text{SMPgAc} = \left(\frac{\Phi_S}{z_2}\right)*100\% \tag{15}$$

Eq. (15) is valid if the light component is not allowed to be present in the solid phase. For set values of z_2 and %SMPgAc, Eq. (15) can be solved for Φ_S and the result plugged into Eq. (12) to obtain the corresponding x_2 value. Table 3 shows also such x_2 values. In Table 3, x_2 decreases as %SMPgAc increases. This agrees with Fig. 2 where it is seen that at set z_2, Φ_S increases as x_2 decreases (notice in Eq. (15) that, at set z_2, the %SMPgAc is proportional to Φ_S.

When looking at Tables 3 to 6, it is clear that a given x_2 value may appear in different tables (see, e.g., rows (5,5′) in Table 3, (1,1′) in Table 4, (0,0′) in Table 5, and (12,12′) in Table 6: $x_2 = 9 \times 10^{-5}$for all such cases). This comes from Eq. (12) which can be graphically represented not only as in Fig. 2 but also as in Fig. 3.

In Fig. 3, we see that a given value of x_2, e.g., $x_2 = 0.3$, is compatible with an infinite number of (z_2, Φ_S) combinations. A given value of x_2 defines an INE. Such INE has degeneracy because its pressure-

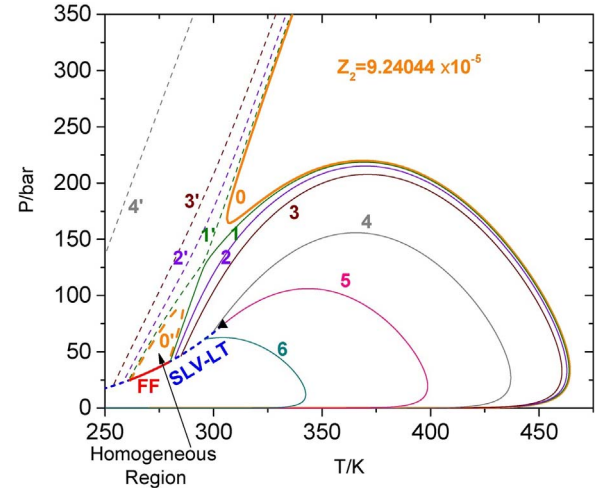

Fig. 9. Computed full isopleth showing SF constant quality curves for the CO_2(1) + MPgAc(2) mixture of global composition $z_2 = z_2'' = 9.24044 \times 10^{-5}$. Labels: see Table 4. Model parameters in Appendix A. See stability analysis in Appendix B. This figure is particularly related to the insert in Fig. 5.

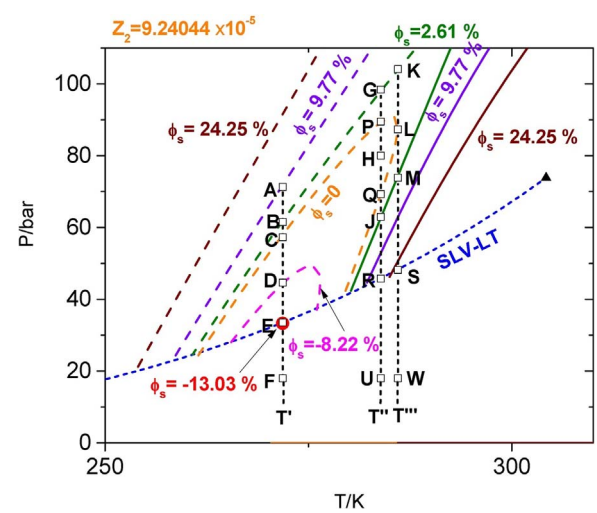

Fig. 10. Zoom of Fig. 9 with the addition of two negative Φ_S level curves.

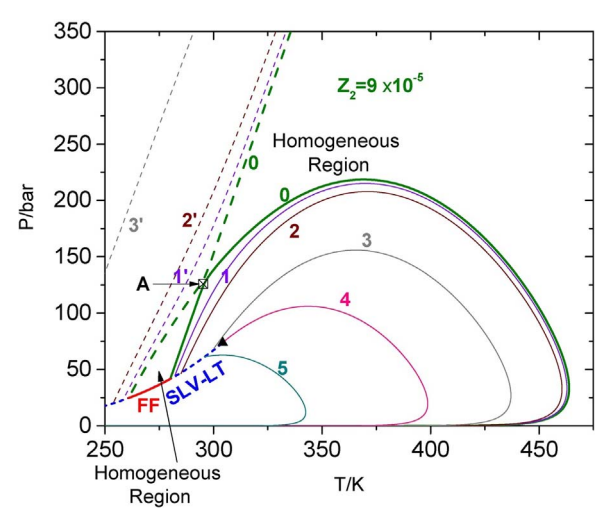

Fig. 11. Computed full isopleth showing SF constant quality curves for the CO_2(1) + MPgAc(2) mixture of global composition $z_2 = z_2''' = 9 \times 10^{-5}$. Labels: see Table 5. Model parameters in Appendix A.

Table 3
Percentage of solidified MPgAc(2) in the mixture with CO_2(1) for Figs. 6 and 7 ($z_2 = z_2^{'}$=0.00014).

Label	% Solidified MPgAc	x_{MPgAc} (= x_2)	Label	% Solidified MPgAc	x_{MPgAc} (= x_2)
0	0	0.00014	10, 10′	99.9999	1.4002×10^{-10}
1	20	1.1200×10^{-4}	11	83.15	2.3588×10^{-5}
2, 2′	25.40	1.0444×10^{-4}	12	99.9990859	1.2799×10^{-9}
3, 3′	28.57	1.0000×10^{-4}	13	99.99999934	9.2678×10^{-13}
4, 4′	34	9.24044×10^{-5}	14	99.99999994	8.3156×10^{-14}
5, 5′	35.72	9.0000×10^{-5}	15	99.99999999	2.0953×10^{-14}
6, 6′	40.45	8.3379×10^{-5}	16	> 99.99999999	3.3640×10^{-16}
7, 7′	50	7.0005×10^{-5}	17	> 99.99999999	7.0495×10^{-17}
8, 8′	92.86	1.0000×10^{-5}	18	> 99.99999999	3.3347×10^{-18}
9, 9′	99.84	2.2867×10^{-7}	19	> 99.99999999	3.9603×10^{-23}

[a] x_{MPgAc} is the medroxiprogesterone acetate mole fraction in the fluid phase of the system. [b] See Eq. (15). [c] $x_2 = 2.2867 \times 10^{-7}$ in level 9-9′ equals the composition of the critical phase of the 1st critical end point (see Fig. 8).

Table 4
Percentage of solidified MPgAc(2) in the mixture for Fig. 9 ($z_2 = z_2^{''}$= 9.24044×10^{-5}. See Appendix B).

Label	% Solidified MPgAc	x_{MPgAc} (= x_2)	Label	% Solidified MPgAc	x_{MPgAc} (= x_2)
	−13.03	1.0444×10^{-4}	3, 3′	24.25	7.0005×10^{-5}
	−8.22	1.0000×10^{-4}	4, 4′	89.18	1.0000×10^{-5}
0	0	9.24044×10^{-5}	5	99.75	2.2867×10^{-7}
1, 1′	2.61	9.0000×10^{-5}	6	99.9998	1.4002×10^{-10}
2, 2′	9.77	8.3379×10^{-5}			

[a] x_{MPgAc} is the medroxiprogesterone acetate mole fraction in the fluid phase of the system. [b] See Eq. (15). [c] $x_2 = 2.2867 \times 10^{-7}$ in level 5 equals the composition of the critical phase of the 1st critical end point (see Fig. 8).

Table 5
Percentage of solidified MPgAc(2) in the mixture with CO_2(1) for Fig. 11 ($z_2 = z_2^{'''}$= 9×10^{-5}).

Label	% Solidified MPgAc	x_{MPgAc} (= x_2)	Label	% Solidified MPgAc	x_{MPgAc} (= x_2)
0	0	9×10^{-5}	3, 3′	88.89	1.0000×10^{-5}
1, 1′	7.36	8.3379×10^{-5}	4	99.75	2.2867×10^{-7}
2, 2′	22.22	7.0005×10^{-5}	5	99.9998	1.4002×10^{-10}

[a] x_{MPgAc} is the medroxiprogesterone acetate mole fraction in the fluid phase of the system. [b] See Eq. (15). [c] $x_2 = 2.2867 \times 10^{-7}$ in level 4 equals the composition of the critical phase of the 1st critical end point (see Fig. 8).

temperature projection (e.g., line 9 in Fig. 6, among other projections) is compatible with different constant Φ_S level curves (indeed of different specified z_2 values, Fig. 3). This degenerated nature of the INEs comes from the assumption of purity for the solid phase.

In Fig. 6, level "0" is the isopleth two-phase envelope (IE, Table 1, line 2). It is of the solid-fluid type in its full extent. Level "1" has a single branch, which is not connected to the SLV curve. Level "2" is the boundary between single-branch levels and double-branch levels. Some branches extend indefinitely towards high pressures and/or towards low temperatures, e.g., branch "3". Some branches have one or two solid-liquid-vapor (SLV) endpoints (e.g. branches 6 and 3′, respectively). To illustrate how the computed level curves can help to understand how a mixture of set overall composition behaves, consider the following set of states. At 100 bar and 475 K, the system is homogeneous. If temperature is decreased at 100 bar, the sequence in Fig. 6 is the following: (0, 1, 2, 3, 4, 5, 6, 7, 8, 9), then (9, 8, 7, 6, 5), and then (5′, 6′, 7′, 8′, 9′, 10′). The sub-sequence (9, 8, 7, 6, 5) is indicative of retrograde behavior. This is so since as temperature decreases the amount of solidified MPgAC decreases; while the 'normal' or intuitive behavior is the opposite, i.e., lower temperature should imply a greater amount of precipitated solid.

The shape of the level curves in Fig. 6 is quite varied: branch 3′ has two SLV points, and branch 3 (same solidified fraction) has none. On the other hand, level (6,6′) has two branches with a single SLV point each.

Clearly, for double branch levels, there is a transition in the topologies of the branches. Such transition happens at a level close to (5,5′) in Fig. 6. The local maximum in pressure of branches such as branch 4′, and the local minimum in pressure of branches such as branch 4 get closer as the %SMPgAc increases. At some%SMPgAc level, such local extrema meet at an "osculation" point where a sort of exchange of semi-branches takes place, giving rise to curves such as those of level (6,6′). For the FI of Figs. 6 and 7, of all solid-liquid branches having one or more SLV points, the one with minimum solidified fraction is the one of level 2′. A level curve branch has at least an SLV point if the solidified fraction is greater than that of level 2 in Fig. 6. Thus, level 2 sets the onset of existence of level curve branches which somewhere loose their stability due to the appearance of a second fluid phase at equilibrium with the already existent fluid and solid phases (SLV point).

Fig. 7 is the same full isopleth of Fig. 6. The differences are that, for Fig. 7, for an easier visualization, the temperature range is slightly

Table 6
Percentage of solidified MPgAc(2) in the mixture with CO_2(1) for Figs. 12 and 13 ($z_2 = z_2^{''''}$= 0.25).

Label	% Solidified MPgAc	x_{MPgAc} (= x_2)	Label	% Solidified MPgAc	x_{MPgAc} (= x_2)
0	0	0.25	9, 9′	99.96866355	1.0444×10^{-4}
1	30.99307669	1.8701×10^{-1}	10, 10′	99.969997	1.0000×10^{-4}
2, 2′	84.18393128	5.0080×10^{-2}	11, 11′	99.97227612	9.24044×10^{-5}
3, 3′	98.49246231	5.0000×10^{-3}	12, 12′	99.97299757	9.0000×10^{-5}
4, 4′	99.42623384	1.9089×10^{-3}	13, 13′	99.97498415	8.3379×10^{-5}
5, 5′	99.6996997	1.0000×10^{-3}	14, 14′	99.97899706	7.0005×10^{-5}
6	99.94974288	1.6750×10^{-4}	15, 15′	99.99699997	1.0000×10^{-5}
7	99.95799412	1.4×10^{-4}	16, 16′	99.9999314	2.2867×10^{-7}
8	99.9663953	1.1200×10^{-4}	17, 17′	99.99999996	1.4002×10^{-10}

[a] x_{MPgAc} is the medroxiprogesterone acetate mole fraction in the fluid phase of the system. [b] See Eq. (15). [c] $x_2 = 2.2867 \times 10^{-7}$ in level 16-16′ equals the composition of the critical phase of the 1st critical end point (see Fig. 8). [d] $x_2 = 5.0080 \times 10^{-2}$ in level 2-2′ equals the composition of the critical phase of the 2nd critical end point (see Figs. 4 and 5).

narrower and also some of the level curves were removed and a number of new ones was added. Fig. 7 presents a greater number of level curves below the SLV curve in comparison to Fig. 6. We see that from a given SLV point, two level curves can stem, e.g., curves 7 and 13; provided that their fluid compositions (liquid and vapor) are compatible with the studied isopleth. This was discussed in a previous section (Table 2) and means that, given the composition of the isopleth (z_2) and that of the analyzed fluid phase ($x_{2,SLV}$ or $y_{2,SLV}$) at three-phase equilibrium, we must obtain a positive solidified fraction, Φ_S (see Eq. (11)). Then, the level curve branch will exist within the solid-fluid region of the studied full isopleth. It is worth noting that both level curve branches stemming from the same SLV point will have different fluid compositions. A special case are branches originating at a CEP (e.g., 1st CEP, branch 9 in Figs. 6 and 7, point 2 in Table 2). The CEP is a SLV point for which phases L and V have become identical (single critical phase). Therefore, only a single branch (not two) stems from such special SLV point. Notice that, for point 2 in Table 2, $x_{2,SLV}$ equals $y_{2,SLV}$, which accounts for the condition of vapor-liquid criticality. Indeed, identical phase compositions lead to identical Φ_S values (Eq. (11)). Point 2 in Table 2 is the 1st CEP.

Since the model does not allow the solidification of CO_2, SF calculations performed at temperatures as low as desired will never result in equilibria with involvement of a pure CO_2 solid phase (notice that the CO_2 melting point is approximately equal to 217 K). Thus, in Fig. 6, some low temperature parts of the calculated level curves, and of the SLV curve are metastable. The level curves that originate at the SLV line in Fig. 7, and exist below it (levels 12–19, Table 3), have Φ_S values extremely close to z_2 (an indeed less than z_2 (in Eq. (14))), and values of the %SMPgAc close to 100% (see Table 3 and see Eq. (15)).

4.2. SLV points of a specified level curve

Having understood the meaning of Figs. 6 and 7, the reader interested in rapidly seeing the variety of qualitative behaviors that the full isopleths of the system under study has, may choose to skip this section on a first reading.

Now we explain how the number of SLV points of a specified level curve is determined (a level curve is specified when z_2 and Φ_S have been set, Eq. (9)). In our approach (based on refs such as ref [3]), this is made once the computed SLV curve is available. The level curve of interest has a $x_2$value given by Eq. (12).

In Fig. 8, where we plot the Pxyz projection of the SLV curves (in the relatively low MPgAc concentration range), the x_2 values associated to the solidification levels of Table 3 (Figs. 6 and 7), or to their INEs, are indicated as vertical dashed lines (DLs). These lines are shown in Fig. 8 for levels 0, 2-2′, 5-5′, 9-9′ and 10-10′ of Figs. 6 and 7.

The number of SLV points, of a specified level curve, equals the number of intersection points between the associated DL and the SLV branches of Fig. 8.

This is because the INE of fluid composition x_2, associated to the level curve of overall composition z_2 and solidified fraction Φ_S, encompasses all equilibria in which one of the fluid phases has a composition equal to x_2, in particular those equilibria involving more than two phases. This condition is met in Fig. 8 at points where a DL intersects a line representing a fluid phase which is at SLV equilibrium with another fluid phase and a solid phase. All SLV points of a DL are SLV points of the corresponding INE and hence of the corresponding level curve.

Since the level 0 DL in Fig. 8 (IE, Table 1, line 2, $x_2 = z_2$ in Table 3) has no intersection points with the SLV-LT locus (see Fig. 8), the IE has a unique SF branch (see Figs. 6 and 7, curve 0) with no contact with the SLV line. Such a unique branch presents a continuous transition from low pressure solid-vapor equilibrium to solid-liquid (or solid-fluid) equilibrium at high pressure.

When Φ_S is increased (x_2 decreases, Fig. 2), starting off at $\Phi_S = 0$, the first DL that intersects the SLV-LT locus in Fig. 8 is the (2,2′) DL (Table 3). Level 2-2′ DL intersects the SLV liquid branch in Fig. 8 tangentially (single intersection point, point 2′ in Figs. 6 and 7). The x_2 value of the 2-2′ DL in Fig. 8 is the maximum x_2 value at which the level curve branches for$z_2 = z_2'$ (Table 3) have SLV points. A maximum x_2 value implies a minimum Φ_S value (Fig. 2) at set z_2 (se also Figs. 6 and 7 and Table 3).

The level 5-5′ DL has two intersection points, i.e, two SLV points. Both happen on the liquid branch of the SLV locus. The existence of two SLV points, for a given solidification level, may give rise to a couple of branches, each originating at one of the two SLV points (e.g., level (6,6′), Fig. 6), or, it may give rise to a single branch having both SLV points as its endpoints (e.g., branch 3′ in Figs. 6 and 7).

Since, for level 5-5′, both intersection points are located on the SLV-LT liquid branch (Fig. 8), branches 5 and 5′ are, at their SLV points, of the liquid-solid type. Hence, both branches initially grow in the region above the SLV-LT line (Figs. 6 and 7). Branch 5′ remains in such region. On the other hand, the nature of branch 5 has a continuous transition from the solid-liquid type to the (low pressure) solid-vapor type (see Figs. 6).

Level 9-9′ DL has two intersection points (Fig. 8). The lowest pressure one is located on the SLV liquid branch. The other intersection point is the 1st CEP, where the liquid and vapor phases at SLV equilibrium become identical, i.e., they actually are a single (critical) phase. The branch that originates at the 1st CEP (branch 9 in Figs. 6 and 7) sets, for branches having one or more SLV points, the boundary that separates branches which are of the SL type at their SLV points (e.g., branch 11 in Fig. 7), from branches of the SV type at their SLV points (e.g., branch 10 in Fig. 7).

Finally, the level 10-10′ DL intersects in Fig. 8 the SLV vapor phase line at higher pressure, and the SLV liquid phase line at lower pressure. Since the nature of the intersection points is different (vapor phase or liquid phase), the intersected SLV points would not simultaneously belong to the same level curve branch. This is shown in Fig. 6: branch 10′ is of the liquid-solid type at its (low temperature) SLV point, while branch 10 is of the solid-vapor type at its (higher temperature) SLV point.

In general, notice that, for this isopleth (i.e, $z_2 = 0.00014$, Figs. 6 and 7), all the level curves with INE fluid composition in between those of the DLs 2-2′ and 9-9′ in Fig. 8, will have, stemming from the SLV-LT curve, a single branch (e.g., 3′ in Fig. 6) or two branches (e.g., 7 and 7′ in Fig. 6), of the liquid-solid type at the originating SLV point. In contrast, the level curves with INE fluid MPgAc mole fraction less than that of the 1st CEP (level 9-9′, Fig. 8) will contain a branch of the solid-liquid type and another branch of the solid-vapor type. Level 2-2′ is a special case since no solid-liquid branch stems from point 2′ in Figs. 6 and 7, i.e., branch 2′ reduces just to a point. This is to say that the solid-liquid branch 2′ has a null length.

4.3. FI of $z_2 = 9.24044 \times 10^{-5}$: the presence of an homogeneity island

Fig. 9 (FI) shows calculated constant Φ_S curves (level curves) for the mixture of global composition $z_2 = 9.24044 \times 10^{-5}$ of the studied system. The labels in Fig. 9 are defined in Table 4. This FI (Fig. 9) has an overall MPgAc concentration less than that of Fig. 6.

Fig. 10 is a zoom of Fig. 9, which also shows a couple of curves with negative solidified fraction. At temperature T', when going from point A to point C (decreasing pressure), Φ_S decreases up to zero. Hence, at point C the system is almost completely made of a fluid phase which is at equilibrium with a disappearing solid phase.

At point D, the negative Φ_S curve to which it belongs indicates than

no solid-fluid equilibrium can exist at the conditions of point D. Thus, at point D there is no solid phase. In general, in continuous constant overall composition processes, during which the number and nature of the involved phases change, the different phases appear or disappear one at a time. Therefore, there would be a single fluid phase at point D. A further pressure reduction takes the system to the SLV equilibrium of point E. The information in Fig. 10 suggests at first sight a transition from a single phase system (point D) to a three-phase system (point E). This is not acceptable since new phases should appear one at a time. There should therefore be an intermediate step at some pressure of the type '1 phase' to '2 phases' transition. Since this would happen at a point (at temperature T') in an area (the one enclosed by the $\Phi_S = 0$ level curve and the SLV curve) where solid-fluid equilibrium cannot exist (because of negative Φ_S values), then, the 1–2 phases transition must be of the fluid–fluid type. These hypotheses are corroborated through a global stability analysis presented in Appendix B. Such analysis was carried out according to Ref. [21].

In conclusion, the sequence in Fig. 10 at T' is the following: SFE (A, B), SFE with zero Φ_S (C), fluid homogeneity (from point C up to some point where a 2nd fluid phase appears), fluid–fluid equilibrium (curve of 2nd fluid phase incipiency not shown in Fig. 10), SLV equilibrium (E) and SVE (F) (and finally: single vapor phase at very low pressure). The 'homogeneous solid' situation is ruled out as long as the overall light component concentration differs from zero: the model does not allow the light component to be present in a solid phase. See more information about Fig. 10 in Appendix C.

4.4. Remarks on the isopleth of Fig. 9

With the previous discussion in mind, and by looking at Fig. 9, we can make the following statements:

- The isopleth in Fig. 9 is of the solid-fluid type in a significant part of its full extent.
- This FI has an homogeneity island delimited by the 0′ line and by a liquid–liquid equilibrium (LLE) line, identified as FF in Fig. 9. This line is located above the SLV-LT line in Fig. 9. This is schematically, more clearly, shown in Fig. B1 in Appendix B.
- The locus where the solid phase is incipient has two branches, i.e., branches 0 and 0′.
- The 0′ level curve has and associated vertical dashed line (see insert in Fig. 5) that intersects the SLV-LT curve twice.
- The level 0 curve is conventionally named 'phase envelope'. This, is more specifically, named 'isopleth two-phase envelope (IE)' in this paper (line 2 in Table 1). This curve has undefined endpoints.
- The level 0′ (SFE) curve, together with the FF (fluid-fluid) curve, wrap an homogeneous region. These two segments are the constitutive parts of an IE, according to our definition of IE (see Table 1, lines 1 and 2). For this reason, the less specific name 'phase envelope', can, in our opinion, also be ascribed to this pair of segments.

Homogeneity islands could bring some confusion when working in the laboratory according to the synthetic method, since, in general, homogeneity is not expected to be found completely surrounded by heterogeneity. This strengthens the general recommendation that the experimentalist should avoid the biased practice of quickly discarding experimental observations that do not seem, at first sight, to be reasonable. In other words: "We are not to tell nature what she's gotta be … She's always got better imagination than we have." [Richard P. Feynman, Nobel Prize in Physics laureate in 1965].

The occurrence of the homogeneity island is related to the existence of two intersection points (see insert in Fig. 5) between the liquid branch of the SLV-LT locus and the DL associated to the global isopleth composition $z_2 = 9.24044 \times 10^{-5}$. However, the existence of two intersection points as those of Fig. 5 does not imply the occurrence of an homogeneity island. For instance the curve 4′ in Fig. 7 (Table 3, level 4-4′, $x_2 = 9.24044 \times 10^{-5}$), is, in the PT plane of Fig. 7, identical to curve 0′ in the PT plane of Fig. 9 (Table 4, level 0, $x_2 = 9.24044 \times 10^{-5}$), however, curve 4′ does not enclose a fluid homogeneity island, at the z_2 value of Fig. 7, while curve 0′ does it in Fig. 9.

Similarly, level zero in Fig. 9 (Table 4) has a PT projection identical to that of level 4 in Fig. 6 (Table 3). This can be clearly seen if we solve Eq. (10) for x_2 after setting z_2 and Φ_S at the values of level zero in Fig. 9 (Table 4) and level 4 in Fig. 6 (Table 3).

According to our modeling results, the system of Fig. 9 is homogeneous at 75 bar and 475 K. When temperature is decreased at 75 bar, the sequence in Fig. 9 is the following: (0, 1, 2, 3, 4, 5) and then (5, 4, 3, 2, 1, 0′). Arriving to level 0′ implies a new homogenous condition within a relatively narrow temperature range (at 75 bar), but a further decrease in temperature promotes a new solidification of MPgAc in the sequence: (0′, 1′, 2′, 3′, 4′). The sub-sequence (5, 4, 3, 2, 1, 0′) is indicative of retrograde behavior. We stress that the homogeneity island is delimited, at its lower pressure side, by a LLE line, which cannot be distinguished, in Fig. 9, from the SLV-LT curve due to the wide ranges of pressure and temperature covered in Fig. 9.

4.5. Coming back to Fig. 1

The overall isopleth composition in Fig. 9 is the same than that in Fig. 1. However, this last figure does not show the homogeneity island detected through the calculation of the level curves (Fig. 9). By comparing Figs. 9 and 1, it is clear that at point 4 in Fig. 1 an homogeneous mixture exists and not an heterogeneous SF one, as originally believed from the sole observation of Fig. 1. This particular case takes us to the conclusion that the computation of constant solidified fraction lines is important not only to estimate the amount of solid phase in the system, but also to detect phenomena that can be regarded as unexpected (e.g., homogeneity islands). In other words, the more complete information provided by the calculated constant solidified fraction curves is helpful to avoid misinterpretations in the study of phase diagrams of systems involving solid phases.

4.6. FI of largest homogeneity island

Fig. 11 is related to the problem of finding the value of z_2 whose FI has the largest homogeneity island. This is explained in Appendix D.

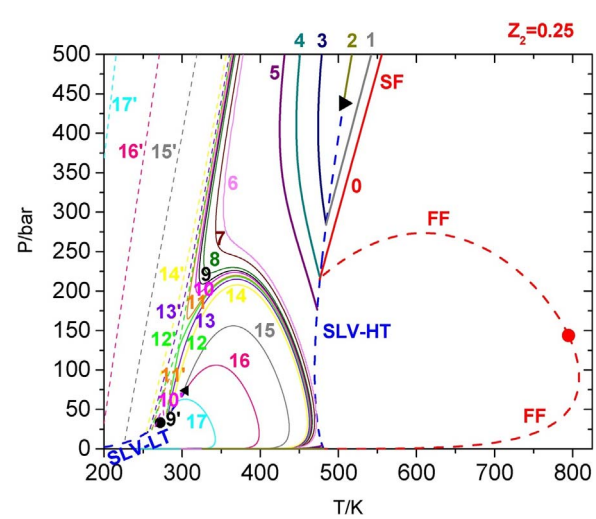

Fig. 12. Computed full isopleth showing SF constant quality curves for the CO_2(1) + MPgAc(2) mixture of global composition $z_2 = z_2^{m} = 0.25$. Labels: see Table 6. Model parameters in Appendix A. Triangles: see Fig. 4. Full red circle: vapor-liquid critical point. (For interpretation of the references to colour in this figure legend, the reader is referred to the web version of this article.)

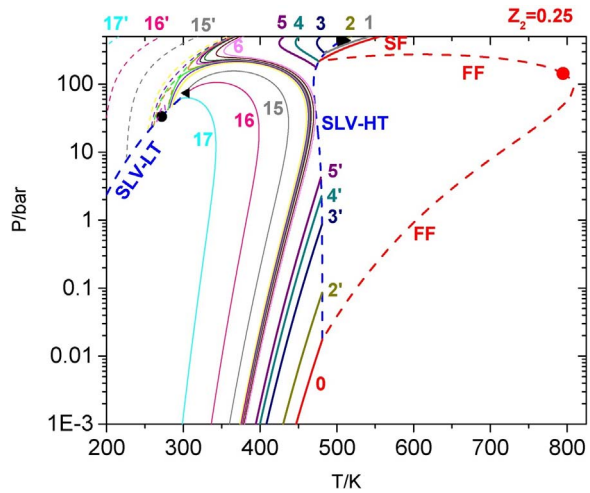

Fig. 13. This figure is the same as Fig. 12 except for the logarithmic scale in the pressure axis.

4.7. A FI of high MPgAc concentration

Fig. 12 presents a FI including the constant quality curves for the CO_2(1) + MPgAc(2) mixture of global composition $z_2 = 0.25$. This mole fraction value falls to the right of that of the 2nd CEP in Fig. 5, i.e., $5.0080 \times 10^{-2} = z_{2,(2ndCEP)} < 0.25$. Fig. 13 is the same as Fig. 12 but in a logarithmic scale, for a better observation of the low pressure region. The labels in Figs. 12 and 13 are defined in Table 6. This isopleth has an overall MPgAc concentration much higher than those of the previously analyzed isopleths (Figs. 6, 9 and 11).

In Fig. 5, a (not shown) vertical line at $z_2 = 0.25$ intersects twice the SLV-HT locus: once on the L(SLV-HT) branch and another time on the V (SLV-HT) branch. The existence of such two intersection points implies in this case that the phase envelope has two solid-fluid segments (level 0 in Figs. 12 and 13). The high-pressure SF segment is easily seen in Fig. 12, and the low-pressure one in Fig. 13.

The phase envelope also has a fluid–fluid (FF) segment with a (LV) critical point (full red circle in Figs. 12 and 13). Notice in Fig. 5 that no INE (constant x_2 value) can have more than a single intersection point with the L(SLV-HT) liquid branch (in contrast with INEs intersecting the L(SLV-LT) locus to the right of the 1st CEP in Fig. 5, e.g., the INE corresponding to the dashed line 5-5′ in Fig. 8). Then, liquid homogeneity islands are not expected for the $z_2 = 0.25$ isopleth.

Fig. 12 shows pairs of level curves that originate at the same SLV point. This is, e.g., the case for level curves 1 and 3: both stem from the same SLV-HT point. This phenomenon was discussed in Section 3.7. At $z_2 = 0.25$, for this SLV-HT point, the compositions of the vapor and liquid phases are both associated to positive Φ_s values [Eq. (10), Table 6]. The phase behavior presented in Fig. 12 is complex and rich. For instance, normal or retrograde solid-fluid behavior is observed depending on pressure, in different isobaric cooling processes. See Appendix C for details.

Isopleths of MPgAc concentration greater than that of Figs. 12 and 13 will have the same qualitative behavior than the one seen in such figures.

Appendix C presents some additional remarks on the results obtained in this work.

5. Conclusions

This work dealt with the phase equilibria involving solid phases of binary, highly asymmetric, systems, as described by a given model with specified parameter values. Close attention was paid to the computation of constant solidified fraction (constant Φ_S) solid-fluid equilibrium lines. In particular, it was proposed a simple criterion to determine the number and nature of constant Φ_S lines that originate at an specific already computed binary solid-liquid-vapor equilibrium point.

The main conclusion is that the detailed description (achieved through several computed constant Φ_S lines) of the 'solid-fluid' region, of a constant overall composition phase diagram, may reveal phenomena which could be regarded as unexpected; in particular, the existence of liquid miscibility islands completely surrounded by heterogeneity regions. These kind of predictions, actually made from a set of experimental data for the system under study (used to fit the model parameters), may help the experimentalist to keep an open mind with regard to the acceptance/rejection of experimentally observed behaviors not matching his/her intuition or previous experience.

In particular, in this work we present, for the system CO_2 + medroxyprogesterone acetate (MPgAc), four computed full isopleths, covering a relatively wide overall composition range (e.g., Fig. 12), which include the phase envelopes, the appropriate segments of the solid-fluid–fluid (SFFE) curves, and several constant solidified fraction curves; the result being a complete portrayal of their solid-fluid regions. The computed constant solidified fraction curves reveal a phase behavior, inside "the supposed to be" solid-fluid region, more complex than the one that would be imagined just from looking at the isopleth phase envelope, and at the appropriate parts of three-phase lines.

Achieving full agreement between the phase equilibria here computed and the real phase behavior of the system under study was not a goal of this work. In spite of that, some readers might find worthwhile to intend to experimentally verify the existence of homogeneity islands for the system CO_2 + medroxyprogesterone acetate, or for other systems of similar nature.

Acknowledgements

We gratefully acknowledge the financial support from the Argentinean institutions: Consejo Nacional de Investigaciones Científicas y Técnicas (CONICET, grant ID: PIP11220150100918), Agencia Nacional de Promoción Científica y Tecnológica (ANPCyT, grant ID: PICT-2012-1998) and Universidad Nacional del Sur (UNS, grant ID: 24/M148).

Appendix A. Parameter values used in this work for the model described in Section 3.1 (taken from Ref. [2]

See Tables A1–A3.

Table A1
Properties of pure compounds [2]

Compound	T_{crit}/ K	P_{crit}/ MPa	ω
CO_2	304.21	7.383	0.223621
Medroxiprogesterone Acetate	851.0	1.316	0.851112

T_{crit} = Critical Temperature. P_{crit} = Critical Pressure. ω = Acentric Factor.

Table A2
Binary interaction parameters [2] for the PR-EoS [7]

System	k_{12} (attractive)	l_{12} (repulsive)
Carbon Dioxide (1) + Medroxiprogesterone Acetate (2)	2.687×10^{-3}	0.1493

Table A3
Medroxiprogesterone Acetate constants [2] for Eq. (5) in the main text.

T_{tp}/ K	481
P_{tp}/ MPa	4.3369×10^{-4}
Δv^{S-L}/ (m^3/kmol)	−0.42551
C_1/ MPa	−150.0
C_2/ MPa	0
C_3/ MPa	0

Appendix B. Stability analysis to confirm that the model predicts an homogeneity island

According to our primary modeling results and conjectures, the system of Fig. 9 of the main text (global MPgAc mole fraction = 9.24044×10^{-5}), presents an homogeneity region delimitated by the curve of level 0′, and by a LLE line (FF line in Fig. 9) at its lower pressure side. This LLE line, at the scale of Fig. 9, cannot be distinguished in Fig. 9 from the SLV-LT curve, due to the wide pressure and temperature ranges covered in Fig. 9. In this appendix we present the results of a stability analysis that we performed following Ref. [21] in order to confirm our conjecture that states that the model predicts the existence of an homogeneity island for the mentioned global composition. By "primary" modeling results we mean those calculation results which do not include the computations corresponding to the stability analysis. Primary calculations are those based on the isofugacity condition which can be coupled to mass conservation conditions. An example of primary result is the Φ_S value of a constant Φ_S curve that originates at a particular SFF equilibrium point.

Fig. B1 shows semi-schematically the homogeneous liquid region (labeled "FLUID") delimitated by the solid-fluid boundary (dashed curve) at its upper end, and by the fluid–fluid boundary (solid curve) at its lower end. Moreover, a solid-fluid–fluid locus (SFF, dotted-dashed curve) is shown at pressures less than those of the FF boundary. A fluid–fluid region is located in between the last mentioned pair of equilibrium lines. The global stability of the system is tested at six different conditions. The temperature is in all cases 270 K. The pressure values (P_1 to P_6) are the indicated in Fig. B1 and in Table B1 where also the results of the stability tests to be discussed below are anticipated. In Fig. B1 we also indicate the pressures P_{FF} and P_{SFF} which correspond to the calculated biphasic fluid–fluid (LLE) and triphasic solid-fluid–fluid (SLV) conditions at 270 K for the studied mixture, respectively.

At the T and P conditions of Fig. B2 (point 1 in Table B1, and point P_1 in Fig. B1) we expected a solid-fluid equilibrium system, then we calculated the SFE conditions (primary computation) and we obtained that a pure MPgAc(2) solid phase was in equilibrium with a fluid phase with $x_2 = 5.968606436 \times 10^{-5}$. Notice that the calculated MPgAc mole fraction for the fluid phase (x_2) was less that the global composition of the system, i.e. $x_2 = 5.968606436 \times 10^{-5} < z_2 = 9.24044 \times 10^{-5} < 1$; consequently, the mass conservation requirement is fulfilled. Next, we performed a stability analysis for the fluid mixture (tested phase) of composition $z_2 = 5.968606436 \times 10^{-5}$ (i.e., for a fluid mixture of composition equal to that of the fluid phase of the calculated SFE). The result is shown in Fig. B2. The continuous curve shows that no trial fluid phase has a relative stability greater than that of the tested phase (which has $z_2 = 5.968606436 \times 10^{-5}$). This is because the tpd (reduced tangent plane distance) is positive for any fluid trial phase. Trivially, at the composition of the tested phase, the tpd should be zero and it should also be minimum (at least locally (see insert)). Both conditions are met by the continuous line in Fig. B2. The tpd of the (pure) solid phase (full circle in Fig. B2) is seen to be zero. Thus, the solid phase is at equilibrium with the tested phase, i.e., with the fluid phase of composition $z_2 = 5.968606436 \times 10^{-5}$. In conclusion, as expected, the globally stable condition for the mixture of $z_2 = 9.24044 \times 10^{-5}$ at T = 270 K and P = P1 = 100 bar is a solid-fluid equilibrium with a fluid phase of composition $z_2 = 5.968606436 \times 10^{-5}$ and a solid phase made of pure MPgAc; the heterogeneous system having finite quantities of either phase (i.e., no phase has a differential size). Notice that according to Fig. 9 (in the main text) this point corresponds to a solid-fluid condition without incipient phases. A (not shown) stability test performed at T = 270 K and P = P1 = 100 bar for a tested fluid phase of the composition ($z_2 = 9.24044 \times 10^{-5}$) of the isopleth of Fig. 9, led to the conclusion that such tested phase is not stable, as expected.

At the conditions of point P_2 in Fig. B1, (point 2 in Table B1) our primary calculations establish that a fluid phase of composition $z_2 = 9.24044 \times 10^{-5}$ is in equilibrium with an incipient pure MPgAc solid phase (this is a point of the 0′ curve in Fig. 9). The stability analysis, for a tested phase equal to the previous fluid phase, is shown in Fig. B3. It is seen that the pure MPgAc solid phase (full circle) has a zero tpd, and that the tpd is positive for all possible fluid non-trivial trial phases. Hence, the solid phase is at equilibrium with the fluid phase of $z_2 = 9.24044 \times 10^{-5}$ as expected. This SFE is the globally stable situation. The tpd analysis of Fig. B3 thus confirms the results of our primary calculations. The incipiency of the solid phase (see Fig. 9 in the main text, 0′ curve) comes from the fact that the overall composition is the same than the composition of the fluid phase at equilibrium with the solid phase (Eq. (11) in main text).

At the conditions of points 3 and 4 in Fig. B1 (and in Table B1), the studied mixture of global composition $z_2 = 9.24044 \times 10^{-5}$ is expected to be a homogeneous fluid. This expectation comes, in part, from the fact that points 3 and 4 are located in a region without constant Φ_S curves having positive Φ_S values. To verify the expectation of homogeneity, we perform a couple of stability tests for a fluid mixture with the mentioned global composition of the system, at the T and P values of points 3 and 4 in Table B1, respectively. Fig. B4 corresponds to point 3 in Table B1 and Fig. B1. Fig. B4 shows a positive tpd for all the possible fluid trial phases. So is the case for the pure solid MPgAc (full circle). Thus, the system of global composition $z_2 = 9.24044 \times 10^{-5}$ at the T and P conditions of point 3 is an homogeneous fluid (no solid phase exists (see also Fig. 9)). This confirms the previously mentioned expectation of homogeneity. The same conclusion is reached through the tpd analysis shown in Fig. B5 for the T and P conditions of point 4 (Table B1 and Fig. B1). A difference between points 3 and 4 (i.e., Figs. B4 and B5 respectively) is that point 4 is closer in

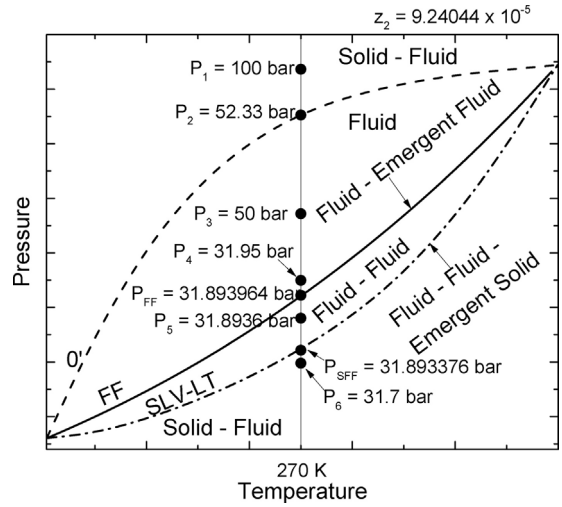

Fig. B1. Schematic diagram of the "homogeneity island" detected for the CO_2 + medroxiprogesterone acetate system with overall mole fraction of MPgAc: $z_2 = z_2'' = 9.24044 \times 10^{-5}$. Notice that the pressures P_1 to P_6 are the pressures of points 1–6 in Table B1, respectively. Dashed line: Solid-Fluid equilibrium boundary of homogeneous region (this is the 0′ curve in Fig. 9). Solid line: Fluid–Fluid (LL) equilibrium boundary of homogeneous region (this is line FF in Fig. 9). Dashed-dotted line: Fluid-Fluid-Solid three-phase equilibrium line (this is line SLV-LT in Fig. 9). This figure is based on primary model computations and conjectures to be confirmed through the stability analysis performed in this Appendix.

Table B1
Tested conditions in the stability analysis performed for the CO_2(1) + medroxiprogesterone acetate(2) system. Model parameters in Appendix A.

PointID	T/K	P/bar	MPgAc mole fraction of the tested phase (z_2)	Figure	Detected globally stable phase condition
1	270	P1 =1 00	$5.968606436 \times 10^{-5}$	Fig. B2	Solid – Fluid
2	270	P2 = 52.33016417	9.24044×10^{-5}	Fig. B3	Solid (incipient) – Fluid
3	270	P3 = 50	9.24044×10^{-5}	Fig. B4	Homogeneous Fluid (Liquid)
4	270	P4 = 31.95	9.24044×10^{-5}	Fig. B5	Homogeneous Fluid (Liquid)
5	270	P5 = 31.8936	$1.687929988 \times 10^{-15}$	Fig. B6	Fluid-Fluid
6	270	P6 = 31.70	$1.682480779 \times 10^{-15}$	Fig. B7	Solid-Fluid

Global composition of the system under study: $x_{CO2} = 0.999907596$, $x_{MPgAc} = 9.24044 \times 10^{-5}$

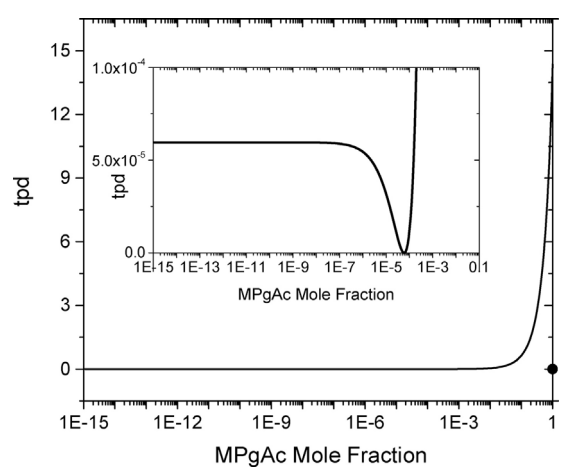

Fig. B2. Reduced tangent plane distance (tpd) vs. mole fraction of MPgAc(2) in the trial phase. MPgAc mole fraction of the tested phase $z_2 = 5.968606436 \times 10^{-5}$. T = 270 K, P = P1 = 100 bar (point 1, Table B1 and point P1 in Fig. B1). Circle: pure solid MPgAc. System: CO_2(1) + MPgAc(2).

pressure to the FFE (Liquid-Liquid, P_{FF}) condition for which one of the two phases is incipient (liquid–liquid cloud point) for the system at such temperature Fig. B1.

Using the adopted model our primary computations led the conditions predicted for the FFE cloud point and the SFFE at 270 K (Fig. B1). Such conditions are the following: a) FFE cloud point: $T = 270$ K, $P_{FF} = 31.893964844748$ bar, $x_2 = 9.24044 \times 10^{-5}$ (set equal to the global MPgAc mole fraction), $y_2 = 1.56368432763470 \times 10^{-15}$ (incipient fluid phase MPgAc mole fracton); b) SFFE: $T = 270$ K, $P_{SFF} = 31.89337625885920$ bar, $x_2 = 1.043387248418340 \times 10^{-4}$, $y_2 = 1.764079668125690.\ 10^{-15}$ (solid phase made of pure MPgAc). This information leads to the expectation of a fluid–fluid equilibrium, as the globally stable situation, at the T,P conditions of point 5 in Table B1 and Fig. B1, for the mixture of overall composition $z_2 = 9.24044 \times 10^{-5}$, since point 5 is located in between the FFE cloud point and the SFFE points.

At the T,P conditions of point P_5, our primary calculations tell that a fluid phase of composition $x_2 = 9.9801 \times 10^{-5}$ is in equilibrium with another fluid phase of composition $y_2 = 1.687929988 \times 10^{-15}$. Notice that for the calculated equilibrium the mass conservation restriction for the mixture is fulfilled, i.e. $y_2 = 1.687929988 \times 10^{-15} < z_2 = 9.24044 \times 10^{-5} < x_2 = 9.9801 \times 10^{-5}$. To verify whether the FF condition is the

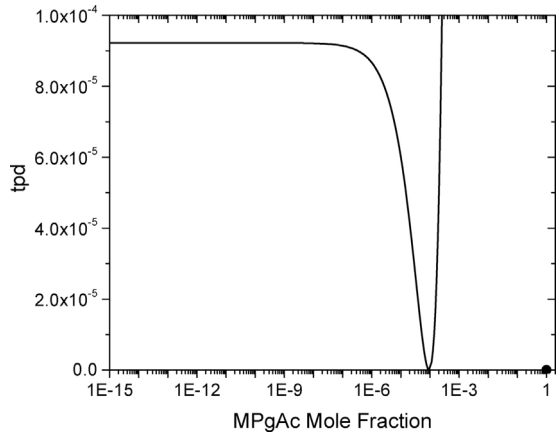

Fig. B3. Reduced tangent plane distance (tpd) vs. mole fraction of MPgAc(2) in the trial phase. MPgAc mole fraction of the tested phase $z_2 = 9.24044 \times 10^{-5}$. T = 270 K, P = P2 = 52.33016417 bar (point 2, Table B1 and point P2 in Fig. B1). Circle: pure solid MPgAc. System: CO_2(1) + MPgAc(2).

globally stable situation, we performed a stability test for a tested fluid mixture of composition equal to that of one of the previously mentioned phases, i.e., $1.687929988 \times 10^{-15}$ MPgAc mole fraction. The stability test results are depicted in . This figure shows a positive tpd for all possible fluid trial phases except for the tested phase and, properly, for the fluid phase of $x_2 = 9.9801 \times 10^{-5}$ for which tpd = 0. Moreover, a positive tpd is encountered in Fig. B6 for the pure MPgAc solid phase (full circle). Thus, point 5 in Table B1 (and in Fig. B1) corresponds to a fluid–fluid condition as the globally stable situation for the mixture of global composition $z_2 = 9.24044 \times 10^{-5}$. Both phases have finite (non-differential) sizes. Thus, as conjectured, a FF condition is the true equilibrium situation for the model. It is worth mentioning that, as seen in Fig. B6, the tpd is extremely close to zero for mixtures of composition close to that of the tested phase (i.e., to $z_2 = 1.687929988 \times 10^{-15}$). The visualization of the ordinate value at the scale of Fig. B6 is very difficult, even in the insert of Fig. B6. In spite of this, we were able to verify, from observing the (not shown here) output numerical tpd values, the presence of a tpd minimum at the low composition of the tested phase.

P_6 in Fig. B1 (point 6 in Table B1) has a pressure (31.7 bar) slightly less than the pressure of the previously mentioned SFFE point (P_{SFF} = 31.89337625885920 bar). Besides, above the SFF (dotted-dashed) curve in Fig. B1 there is a FF region. For such two reasons, the expected phase condition at the T and P of P_6 for the mixture of $z_2 = 9.24044 \times 10^{-5}$ is solid-fluid equilibrium.

For the *T* and *P* conditions of point P_6 we obtained, from primary computations, that a pure solid MPgAc phase was in equilibrium with a fluid phase of $z_2 = 1.682480779 \times 10^{-15}$.

Once again, notice that the MPgAc mole fraction calculated for the fluid phase is less that the global MPgAc mole fraction, i.e. $z_2 = 1.682480779 \times 10^{-15} < z_2 = 9.24044 \times 10^{-5} < 1$; consequently, the mass conservation requirement is again fulfilled.

Following the same procedure of previous cases, we again performed a stability analysis, this time for the a tested phase of composition $z_2 = 1.682480779 \times 10^{-15}$. We encountered a tpd equal to zero for the tested phase and also for the pure MPgAc solid phase, as expected, and found that the tpd remained positive for all possible trial fluid phases (see Fig. B7). Thus, a globally stable solid-fluid equilibrium condition was verified for point 6, which confirmed the expectations, i.e., SFE. In this case, it is also observed (Fig. B7) that the tpd approaches a zero value for the mixtures with a MPgAc mole fraction close to that of the tested phase, as it happens for point 5 in Fig B6.

In conclusion, the stability tests carried out in this Appendix confirm that the model predicts the existence of an homogeneity island (of the liquid type) at overall composition $z_2 = 9.24044\ 10^{-5}$, and they also confirm that the evolution conjectured for the phase condition when going from point P1 to P6 in Fig. B1 is the correct one. Notice that the composition conditions for the tested phase is also reported in Table B1.

To fix ideas, we now summarize the strategy applied in the present Appendix. Depending on the expected condition for the system, we proceed as follows:

a) For the cases where an homogeneous system was expected, at the T and P established (points 3 and 4, and Figs. B4 and B5 respectively), the

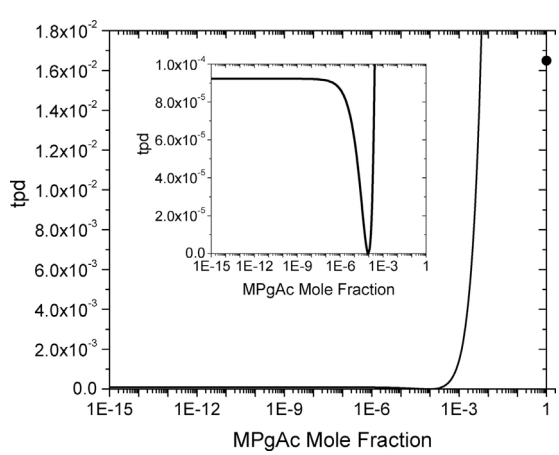

Fig. B4. Reduced tangent plane distance (tpd) vs. mole fraction of MPgAc(2) in the trial phase. MPgAc mole fraction of the tested phase $z_2 = 9.24044 \times 10^{-5}$. T = 270 K, P = P3 = 50 bar (point 3, Table B1 and point P3 in Fig. B1). Circle: pure solid MPgAc. System: CO_2(1) + MPgAc(2).

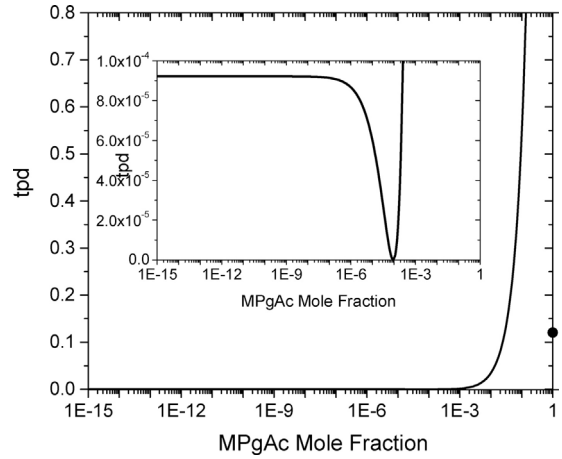

Fig. B5. Reduced tangent plane distance (tpd) vs. mole fraction of MPgAc(2) in the trial phase. MPgAc mole fraction of the tested phase $z_2 = 9.24044 \times 10^{-5}$. T = 270 K, P = P4 = 31.95 bar (point 4, Table B1 and point P4 in Fig. B1). Circle: pure solid MPgAc. System: CO_2(1) + MPgAc(2).

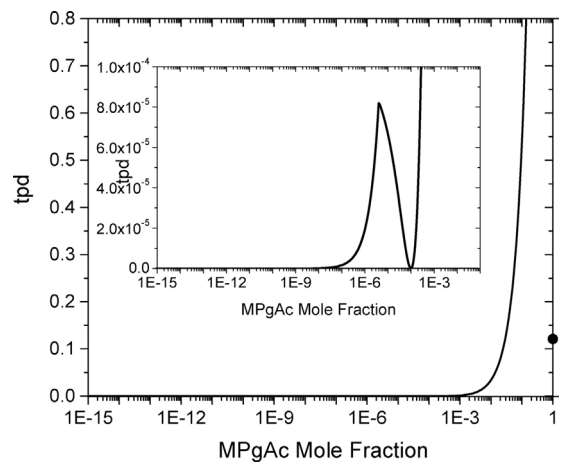

Fig. B6. Reduced tangent plane distance (tpd) vs. mole fraction of MPgAc(2) in the trial phase. MPgAc mole fraction of the tested phase $z_2 = 1.687929988 \times 10^{-15}$. T = 270 K, P = P5 = 31.8936 bar (point 5, Table B1 and point P5 in Fig. B1). Circle: pure solid MPgAc. System: CO_2(1) + MPgAc(2).

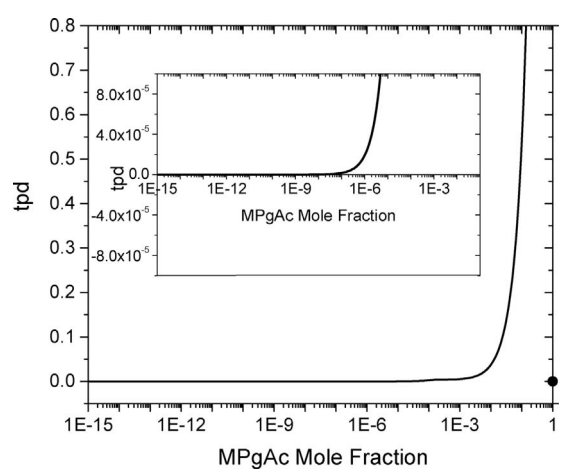

Fig. B7. Reduced tangent plane distance (tpd) vs. mole fraction of MPgAc(2) in the trial phase. MPgAc mole fraction of the tested phase $z_2 = 1.682480779 \times 10^{-15}$. T = 270 K, P = P6 = 31.7 bar (point 6, Table B1 and point P6 in Fig. B1). Circle: pure solid MPgAc. System: CO_2(1) + MPgAc(2).

composition of the tested phase considered was the global composition of the isopleth in Fig. 9 ($z_2 = 9.24044 \times 10^{-5}$).

b) When a solid-fluid equilibrium with an incipient solid phase was expected (point 2, Fig. B3), the solid-fluid equilibrium pressure (and other variables) was computed (isofugacity condition) at the specified temperature and at a fluid phase composition equal to the isopleth global one. Next, a stability analysis was performed at the set temperature and at a pressure equal to the previously computed one, with the composition of the tested phase again set equal to the global composition of the isopleth.

c) For the cases where an heterogeneous condition (SF or FF) with phases of finite size was expected, we first calculated (isofugacity condition) the biphasic equilibrium phase compositions (and other variables) at the T and P established. Next, we verified that the mass conservation requirement was satisfied by the equilibrium point obtained. Finally, we performed the stability test for the system, setting the composition of the tested phase equal to the previously computed composition of one of the two phases, either to that of the only fluid phase in solid-fluid equilibrium, or to that of one of the fluid phases for the case of fluid–fluid equilibrium. Thereby, we first look, through primary calculations, for the biphasic equilibrium at the temperature and pressure conditions established (solid-fluid equilibrium for points 1 and 6, and fluid–fluid equilibrium for point 5), and then we confirm the global stability of the supposed two-phase condition through the stability analysis of the tested phase (see Figs. B2 and B7 and Fig. B6 respectively).

Appendix C. Some remarks

Degeneracy of PT projections of constant Φ_S curves

From Eq. (12) we observe that there would be an infinite number of combinations of z_2 and Φs values that render the same x_2 (Fig 3). Then, the PT projection will remain the same for level zero curve in Fig. 9 ($z_2 = 9.24044 \times 10^{-5}$, Table 4) and level 4 curve in Fig. 6 ($z_2 = 0.00014$, Table 3), i.e, in the PT plane they will be equal. However, the solidified fractions of both curves will be different. In terms of percentage of solidified MPgAc in the mixture according to Tables 4 and 3, level zero in Fig. 9 corresponds to 0% of MPgAc (i.e., $\Phi_S = 0$, Table 4) and level 4 in Fig. 6 to 34 % of MPgAc (i.e., $\Phi_S = 4.76E\text{-}5$, Table 3). Once again, notice that the set of variables in Eqs. (1) to (3) does not include the relative amounts of the fluid and solid phases in the system.

Fig 10: Another couple of pressure reduction processes at $z_2 = 9.24044\ 10^{-5}$

A second pressure reduction process at temperature T" in Fig. 10, which connects points G and U, follows the sequence: SFE (G), SFE at zero Φ_S (point P), single fluid phase (H), SFE at zero Φ_S (Q), SFE (J), SLV equilibrium (R), and SVE (U). The process a T" has no fluid–fluid transition, while that at T' does. Otherwise, the single fluid phase range at T" is bounded by two SFE points (P and Q) with an incipient solid phase, while the homogeneous fluid range at T' is bounded by a SFE point (C) with an incipient solid phase, and a fluid–fluid point (not shown in Fig. 10). At T"', a zero Φ_S point (L) is reached only once, i.e., at T"', the homogeneity range is at the verge of its disappearance. Notice that, at point L, the vertical line at T"' meets the zero Φ_S curve tangentially, i.e., a tiny reduction or increase in pressure, with respect to that of point L, makes the size of the solid phase go from zero to a positive value. This behavior would also be found for any curved path in the PT plane meeting the zero Φ_S curve of Fig 10 tangentially.

About Figs. 12 and 13

For the system of Fig. 12, at 450 bar and 600 K, the system is homogeneous. If temperature is decreased at 450 bar, the sequence in Fig. 12 is the following: (0, 1, 2, 3, 4, 5, 6, 7, 8, 9, 10, 11, 12′, 13′, 14′, 15′,16′, 17′) with a continuous increase in the MPgAc solidified fraction (see Table 6). Thereby, a normal (non retrograde) behavior with respect to temperature at 450 bar is observed for the mixture in Fig 12.

In Fig 12, at 250 bar and 800 K, the system is homogeneous, and diminishing temperature at constant pressure, a fluid–fluid (FF, bubble point) boundary is reached (retrograde liquid-vapor behavior). Then, if we continue reducing temperature, a FF heterogeneous system is observed until a new FF (again bubble point) boundary is reached at approximately 525 K. With a further decrease of T, a fluid homogeneous condition is obtained until a solid phase appears when the (level 0) SF line is crossed. From that point, the sequence is the following: (0, SLV-HT curve, 4, 5, 6, 7, 8, 9, 10, 11, 12′, 13′, 14′, 15′, 16′, 17′). Notice that we did not intend to characterize the fluid–fluid region of this isopleth. This would be done by computing a set of constant liquefied fraction lines (I-C-FPF-L, Table 1, line 5).

For the system of $z_2 = 0.25$ (Fig. 12), at 100 bar and 850 K a homogeneous mixture exists. If temperature is decreased at constant pressure a FF line (dew curve) is crossed and a second (incipient) fluid phase appears (liquid). A further decrease in T occurs in the presence of two fluid phases, until a SLV-HT is reached where a pure MPgAc solid phase also appears. From that point, a reduction in temperature a constant P induces the following sequences of solid-fluid states: (6, 7, 8, 9, 10, 11, 12, 13, 14, 15, 16), then (16, 15, 14, 13, 12) and then, (12′, 13′, 14′, 15′, 16′). Thus, for this mixture, at 100 bar, a solid-fluid retrograde behavior is detected (sequence 16, 15, 14, 13, 12).

Finally, in the low pressure region, at 0.01 bar and 500 K (see Fig. 13), an homogenous vapor mixture is observed. Then, by reducing T at constant P, a solid phase appears at level 0, and the observed sequence is: (0, 2′, 3′, 4′, 5′, 6, 7, 8, 9, 10, 11, 12, 13, 14, 15, 16, 17), indicating a normal behavior with respect to temperature for the studied system at 0.01 bar.

Binary solid-fluid master diagram

In principle, it would be possible to generate a sort of binary solid-fluid master diagram (SF-MD), in the PT plane, that would be made of a large enough number of computed INEs, covering the x_2 range of interest. Notice that this diagram would be obtained without ever specifying values for variables z_2 and Φ_S. Then, for studying a FI of specified z_2, one would just remove from the SF-MD all INE branches giving, according to Eq. (11), negative Φ_S values. The resulting diagram would not provide complete information but it would anyway give, at a glance, valuable information on the behavior predicted for the system.

This SF-MD is unique for a given binary system, once the model and its parameters values have been specified. This uniqueness is due to the assumption of total absence of the light component in the solid phase.

If the Arabic numbers used as curve labels in Fig. 12, and also both FF curves, were all removed, then, the resulting chart would be a SF-MD to be

used for FIs with $z_2 \leq 0.25$

Appendix D. Identification of the full isopleth of largest homogeneity island

Fig. 11 shows the full isopleth for the CO_2(1) + MPgAc(2) mixture of global composition $z_2 = 9\ 10^{-5}$. The level curve labels are defined in Table 5. The IE (Table 1) has two SF segments (level 0 (0 dashed curve and 0 solid curve)), and a FF one (of LLE type). Each IE SF segment has an intersection point with the SLV-LT curve (as it is the case for the 0′ SF segment of the IE of the FI of Table 4/ Fig. 9, see inset in Fig. 5). In Fig. 11, both IE (0 level) SF segments are close to meet at a point. This is point A in Fig. 11. In what follows, we will assume that they exactly meet at point A.

Level zero in Fig. 11 has a PT projection identical to that of level 5-5′ in Fig. 6 and of level 1-1′ in Fig. 9. As seen in Tables 3–5, all this level curves correspond to the INE of $x_2 = 9 \times 10^{-5}$. From Fig. 6, it is clear that this INE is a special one: solidification levels higher than 5 are characterized by two branches, each having a single SLV point (e.g., curves 6 and 7 in Fig. 6); while solidification levels lower than 5 have both SLV points within the same branch (e.g., curve 4′), being the other branch (e.g., curve 4) not connected with the SLV line.

The global composition z_2 that makes a given branch of an INE (known x_2), such as branch 4′ in Fig. 6, become the boundary of an homogeneity island, is obtained by setting $\Phi_S = 0$ in Eq. (10) at the known INE x_2 value. The result is $z_2 = x_2$. In Fig. 6 it can be seen that if $\Phi_S = 0$ is imposed on the INE of level (5,5′), then, the corresponding global composition z_2 will be the one of the full isopleth with the largest homogeneity island.

The FI in Fig. 11, which has $z_2 = 9\ 10^{-5}$ which is lower than $z_2 = 9.24044 \times 10^{-5}$ of Fig. 9 (i.e., its composition is closer to that of the 1st CEP in Figs. 5 and 8, which equals 2.2867×10^{-7}), is the one with the homogeneity island of highest size (in the PT plane).

The x_2 value of point A in Fig. 11 is the x_2 value of the curve of level 0 in Fig 11, i.e., (see Table 5) $x_2 = 9 \times 10^{-5}$. It is the minimum FI z_2 value at which a fluid homogeneity island can exist. For instance, a higher z_2 value, e.g., equal to the $x_2$value of the INE (4,4′) in Fig. 6 ($x_2 = 9.24044 \times 10^{-5}$), has an associated FI (the one of Fig. 9) which presents a fluid homogeneity island. However, from looking at Fig. 6, we conclude that if z_2 is greater than the x_2 value of curve (2,2′) ($x_2 = 1.0444 \times 10^{-4}$) no homogeneity island is to be found. The absence of an homogeneity island is also true for level (6,6′) in Fig. 6 and higher levels.

In conclusion, for the present case study, homogeneity islands are found in a range of FI overall compositions, i.e., if z_2 is too low or too high this phenomenon is not observed.

About point A in Fig. 11

Point A in Fig. 11 is a sort of double constant Φ_S point, since it simultaneously belongs to two different branches of the same INE. It seems that point A is unique for a given binary system, i.e., it is an invariant point (zero degrees of freedom).

If the mathematical conditions, valid at point A, were known, then, they could be solved for all the variables of the corresponding system of equations. This would lead, in particular, to the value of x_2 at point A (x_{2_A}). The overall composition $z_2 = x_{2_A}$ is the global composition threshold of existence of fluid homogeneity islands. There could be no solution for the system of equations of point A. In such a case, no such islands would be, in principle, expected.

More on Fig. 11

At 75 bar and 475 K, the system in Fig. 11 is homogeneous. Decreasing temperature at constant P, the observed sequence in Fig. 11 is: (0, 1, 2, 3, 4) and then (3, 2, 1, 0). At level 0 an homogeneous condition exists, which extends for some degrees at 75 bar. A further decrease in T promotes a new solidification of MPgAc in the sequence (0, 1′, 2′, 3′). The sub-sequence (3, 2, 1, 0) indicates the existence of retrograde behavior for this mixture at 75 bar.

Reference

[1] W.M. Giufrida, S.B. Rodriguez-Reartes, C.G. Alonso, M.S. Zabaloy, V.F. Cabral, F.W. Tavares, L. Cardozo-Filho, High-pressure experimental data of CO2 + Mitotane and CO2 + Ethanol + Mitotane mixtures, J. Chem. Eng. Data 56 (2011) 4333–4341.

[2] L.F. Pinto, S.B. Rodriguez-Reartes, M.L. Corazza, V.F. Cabral, P.H.H. de Araújo, E.H. Madureira, M.S. Zabaloy, L. Cardozo-Filho, Phase behavior of carbon dioxide + medroxyprogesterone acetate system at high pressures, Fluid Phase Equilib. 349 (2013) 1–11.

[3] S.B. Rodriguez-Reartes, M. Cismondi, E. Franceschi, M.L. Corazza, J.V. Oliveira, M.S. Zabaloy, High-pressure phase equilibria of systems carbon dioxide + n-eicosane and propane + n-eicosane, J. Supercrit. Fluids 50 (2009) 193–202.

[4] S.B. Rodriguez-Reartes, G.O. Pisoni, M.S. Zabaloy, Test for the detection of the retrograde melting phenomenon in computed solid–fluid equilibria of binary asymmetric systems, J. Supercrit. Fluids 97 (2015) 36–44.

[5] M. Škerget, Ž. Knez, M. Knez-Hrnčič, Solubility of solids in sub- and supercritical fluids: a review, J. Chem. Eng. Data 56 (2011) 694–719.

[6] C.B. Kautz, G.M. Schneider, J.-J. Shim, B. Wagner, D. Tuma, Solubilities of a 1,4-Bis (alkylamino)-9,10-anthraquinone series in compressed carbon dioxide, J. Chem. Eng. Data 53 (2008) 2356–2371.

[7] D.-Y. Peng, D.B. Robinson, A new two-Constant equation of state, Ind. Eng. Chem. Fundam. 15 (1976) 59–64.

[8] A. Diefenbacher, M. Türk, Phase equilibria of organic solid solutes and supercritical fluids with respect to the RESS process, J. Supercrit. Fluids 22 (2002) 175–184.

[9] A. Firoozabadi, Thermodynamics of Hydrocarbon Reservoirs, 1st ed., McGraw-Hill, 1999.

[10] J.M. Prausnitz, Molecular Thermodynamics of Fluid-Phase Equilibria, 1st ed., Prentice-Hall Inc., Englewood Cliffs, New Jersey. USA, 1969.

[11] J. Wisniak, A. Apelblat, H. Segura, Prediction of gas-solid equilibrium using equations of state, Fluid Phase Equilib. 147 (1998) 45–64.

[12] S.B. Rodriguez-Reartes, M. Cismondi, M.S. Zabaloy, Modeling approach for the high pressure solid-fluid equilibrium of asymmetric systems, Ind. Eng. Chem. Res. 50 (2011) 3049–3059.

[13] R. Privat, R. Gani, J.-N. Jaubert, Are safe results obtained when the PC-SAFT equation of state is applied to ordinary pure chemicals? Fluid Phase Equilib. 295 (2010) 76–92.

[14] A. Yokozeki, Analytical equation of state for solid-Liquid-Vapor phases, Int. J. Thermophys. 24 (2003) 589–620.

[15] J.M. Smith, H.C. Van Ness, M.M. Abbott, Introduction to Chemical Engineering Thermodynamics, 6th ed., McGraw-Hill Edition, New York, 2003.

[16] G. Pisoni, M. Cismondi, L. Cardozo-Filho, M.S. Zabaloy, Generation of characteristic maps of the fluid phase behavior of ternary systems, Fluid Phase Equilib. 362 (2014) 213–226.

[17] S.B. Rodriguez-Reartes, M. Cismondi, M.S. Zabaloy, Computation of solid–fluid–fluid equilibria for binary asymmetric mixtures in wide ranges of conditions, J. Supercrit. Fluids 57 (2011) 9–24.

[18] M. Cismondi, M.L. Michelsen, M.S. Zabaloy, Automated generation of phase diagrams for supercritical fluids from equations of state. Theory & Thermodynamics., in: 1th European Meeting on Supercritical Fluids., Barcelona-Spain., 2008, pp. Work 192. USB-DRIVE proceedings: OC_TT_197. pdf.

[19] S. Yamamoto, K. Ohgaki, T. Katayama, Phase behavior of binary mixtures of indole or quinoxaline with CO2, C2H4, C2H6, and CHF3 in the critical region, J. Supercrit. Fluids 2 (1989) 63–72.

[20] C.H. Whitson, M.L. Michelsen, The negative flash, Fluid Phase Equilib. 53 (1989) 51–71.

[21] M.L. Michelsen, J.M. Mollerup, Thermodynamic Models: Fundamentals and Computational Aspects, 1st ed., Tie-Line Publications, Denmark, 2004.